

₁ Study of neutrino-nucleus interaction at around 1 GeV using
₂ a 3D grid-structure neutrino detector, WAGASCI, muon
₃ range detectors and magnetized spectrometer, Baby MIND,
₄ at J-PARC neutrino monitor hall

₅ A. Bonnemaison, R. Cornat, L. Domine, O. Drapier, O. Ferreira, F. Gastaldi,
₆ M. Gonin, J. Imber, M. Licciardi, F. Magniette, T. Mueller, L. Vignoli, and O. Volcy
₇ *Ecole Polytechnique, IN2P3-CNRS, Laboratoire Leprince-Ringuet, Palaiseau,*
₈ *France*

₉ S. Cao and T. Kobayashi

₁₀ *High Energy Accelerator Research Organization (KEK), Tsukuba, Ibaraki, Japan*

₁₁ M. Khabibullin, A. Khotjantsev, A. Kostin, Y. Kudenko, A. Mefodiev, O. Mineev,
₁₂ S. Suvorov, and N. Yershov

₁₃ *Institute for Nuclear Research of the Russian Academy of Sciences, Moscow, Russia*

₁₄ B. Quilain

₁₅ *Kavli Institute for the Physics and Mathematics of the Universe (WPI), The*
₁₆ *University of Tokyo Institutes for Advanced Study, University of Tokyo, Kashiwa,*
₁₇ *Chiba, Japan*

₁₈ T. Hayashino, A. Hiramoto, A.K. Ichikawa, K. Nakamura, T. Nakaya, K Yasutome,
₁₉ and K. Yoshida

₂₀ *Kyoto University, Department of Physics, Kyoto, Japan*

₂₁ Y. Azuma, J. Harada, T. Inoue, K. Kin, N. Kukita, S. Tanaka, Y. Seiya,
₂₂ K. Wakamatsu, and K. Yamamoto

₂₃ *Osaka City University, Department of Physics, Osaka, Japan*

24 A. Blondel, F. Cadoux, Y. Favere, E. Noah, L. Nicola, and S. Parsa

25 *University of Geneva, Section de Physique, DPNC, Geneva, Switzerland*

26 N. Chikuma, F. Hosomi, T. Koga, R. Tamura, and M. Yokoyama

27 *University of Tokyo, Department of Physics, Tokyo, Japan*

28 Y. Hayato

29 *University of Tokyo, Institute for Cosmic Ray Research, Kamioka Observatory,
30 Kamioka, Japan*

31 Y. Asada, K. Matsushita, A. Minamino, K. Okamoto, and D. Yamaguchi

32 *Yokohama National University, Faculty of Engineering, Yokohama, Japan*

33 December 14, 2017

34 **Contents**

35 **1 Introduction**

36 The understanding of neutrino-nucleus interactions in the 1 GeV energy region is critical
37 for the success of accelerator-based neutrino oscillation experiments such as the T2K exper-
38 iment. Complicated multi-body effects of nuclei render this understanding difficult. The
39 T2K near detectors have been measuring these and significant progress has been achieved.
40 However, the understanding is still limited. One of the big factors preventing from full
41 understanding is the non-monochromatic neutrino beam spectrum. Measurements with
42 different but some overlapping beam spectra would greatly benefit to resolve the contri-
43 bution from different neutrino energies. We, the Wagasci collaboration, proposes to study
44 the neutrino-nucleus interaction at the B2 floor of the neutrino monitor building, where
45 different neutrino spectra can be obtained due to the different off-axis position. Our exper-
46 imental setup contains 3D grid-structure plastic-scintillator detectors filled with water as
47 the neutrino interaction target (Wagasci modules), two side- and one downstream- muon
range detectors(MRD's). The 3D grid-structure and side-MRD's allows a measurement of

49 wider-angle scattering than the T2K off-axis near detector (ND280). High water to scintil-
50 lator material ratio enables the measurement of the neutrino interaction on water, which
51 is highly desired for the T2K experiment because it's far detector, Super-Kamiokande,
52 is composed of water. The MRD's consist of plastic scintillators and iron plates. The
53 downstream-MRD, so called the Baby MIND detector, also works as a magnet and pro-
54 vides the charge identification capability as well as magnetic momentum measurement for
55 high energy muons. The charge identification is essentially important to select antineu-
56 trino events in the antineutrino beam because contamination of the neutrino events is as
57 high as 30%. Most of the detectors has been already constructed. The Wagasci modules
58 have been commissioned as the J-PARC T59 experiment and the Baby MIND detector was
59 commissioned at the CERN neutrino platform. Therefore, the collaboration will be ready
60 to proceed to the physics data taking for the T2K beam time in January 2019. We will
61 provide the cross sections of the charged current neutrino and antineutrino interactions on
62 water with slightly higher neutrino energy than T2K ND280 with wide angler acceptance.
63 When combined with ND280 measurements, our measurement would greatly improve the
64 understanding of the neutrino interaction at around 1 GeV and contribute to reduce one
65 of the most significant uncertainty of the T2K experiment.

66 **2 Experimental Setup**

67 Figure. ?? and ?? show a schematic view and a CAD drawing of the entire set of detectors.
68 Central neutrino target detectors consist of two Wagasci modules and T2K INGRID proton
69 module. Inside the Wagasci module, plastic scintillator bars are aligned as a 3D grid-like
70 structure and spaces in the structure are filled with water for a water-in Wagasci module.
71 T2K INGRID proton module is a full active neutrino target detector which is composed
72 only with scintillator bars in its tracking region. The central detectors are surrounded by
73 two side- and one downstream- muon range detectors(MRD's) The MRD's are used to select
74 muon tracks from the charged-current (CC) interactions and to reject short tracks caused by
75 neutral particles that originate mainly from neutrino interactions in material surrounding
76 the central detector, like the walls of the detector hall, neutrons and gammas, or neutral-
77 current (NC) interactions. The muon momentum can be reconstructed from its range
78 inside the detector. The MRD's consist of plastic scintillators and iron plates. In addition,
79 each of the iron plates of the downstream-MRD, so called the Baby MIND detector, is
80 wound by a coil and can be magnetized. It provide the charge selection capability.

81 For all detectors, scintillation light in the scintillator bar is collected and transported
82 to a photodetector with a wavelength shifting fiber (WLS fiber). The light is read out by
83 a photodetector, Multi-Pixel Photon Counter (MPPC), attached to one end of the WLS
84 fiber. The signal from the MPPC is read out by the dedicated electronics developed for the
85 test experiment to enable bunch separation in the beam spill. The readout electronics is
86 triggered using the beam-timing signal from MR to synchronize to the beam. The beam-

87 timing signal is branched from those for T2K, and will not cause any effect on the T2K
88 data taking.

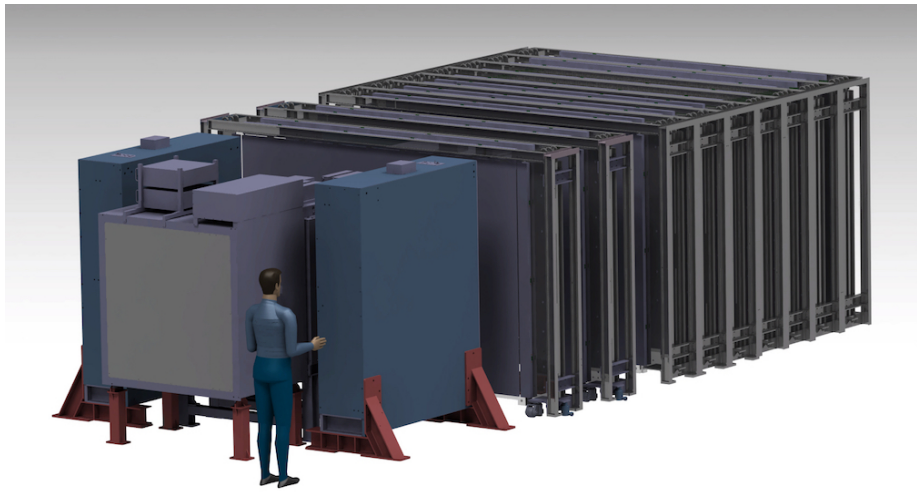


Figure 1: Schematic view of entire sets of detectors.

89 T2K adopted the off-axis beam method, in which the neutrino beam is intentionally
90 directed 2.5 degrees away from SK producing a narrow band ν_μ beam. The off-axis near
91 detector, ND280, is installed towards the SK direction in the B1 floor of the near detector
92 hall of the J-PARC neutrino beam-line. We propose to install our detector in the B2
93 floor of the near detector hall, where the off-axis angle is similar but slightly different: 1.5
94 degree. The candidate detector position in the B2 floor is shown in Fig. ???. The expected
95 neutrino energy spectrum at the candidate position is shown in Fig. ???.

96 **2.1 Wagasci modules**

97 **2.1.1 Main detector**

98 The WAGASCI modules are mainly composed of 1280 plastic scintillator bars and a sur-
99 rounding stainless steel tank as shown in Fig. ???. The total number of channels in one
100 Wagasci module is 1280. The stainless steel tank is constructed by welding stainless steel
101 plates, is sized as $46 \times 125 \times 125$ cm³, and weighs 0.5 ton.

102 One Wagasci module consists of 16 scintillator tracking planes, where each plane is an
103 array of 80 scintillator bars fixed with ABS frames. The 40 bars, called parallel scintillators,
104 are placed perpendicularly to the beam, and the other 40 bars, called grid scintillators, are
105 placed in parallel to the beam with grid structure in the tracking plane as shown in Fig.
106 ???. Thanks to the 3 D grid-like structure of the scintillator bars, the Wagasci module has

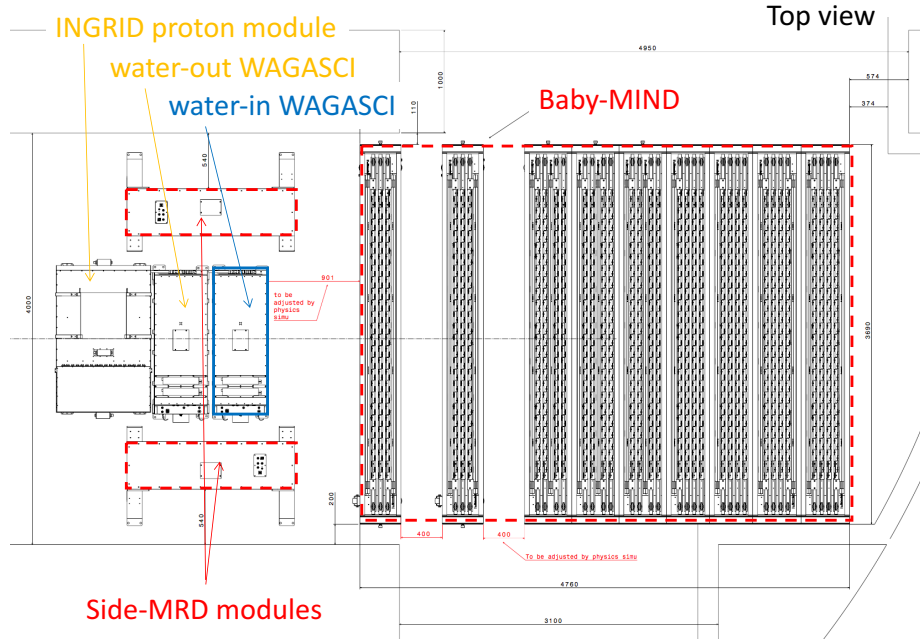


Figure 2: Top view of entire sets of detectors.

¹⁰⁷ 4π angular acceptance for charged particles.

¹⁰⁸ Thin plastic scintillator bars produced at Fermilab by extrusion method, mainly consists
¹⁰⁹ of polystyrene and are surrounded by thin reflector including TiO² (3 mm in thickness)
¹¹⁰ are used for the Wagasci modules to reduce the mass ratio of scintillator bars to water,
¹¹¹ because neutrino interactions in the scintillator bars are a background for the cross section
¹¹² measurements on H₂O. Each scintillator bar is sized as 1020×25×3 mm³ including the
¹¹³ reflector part, and half of all the scintillator bars have 5-cm-interval slits to form the grid
¹¹⁴ structure (Figure ??).

¹¹⁵ We will have two types of the Wagasci modules, a water-in module and a water-out
¹¹⁶ module. The water-in Wagasci module has water in spaces of the grid structure. The total
¹¹⁷ water mass serving as neutrino targets in the fiducial volume of the module is 188 kg, and
¹¹⁸ the mass ratio of scintillator bars to water is 80 %. The water-out Wagasci module doesn't
¹¹⁹ have water inside the detector. The total CH mass serving as neutrino target in the fiducial
¹²⁰ volume of the module is 47 kg, and the mass fraction of scintillator bars is 100 %.

¹²¹ Scintillation light is collected by wave length shifting fibers, Y-11 (non-S type with a
¹²² diameter of 1.0 mm produced by Kuraray. A fiber is glued by optical cement in a groove
¹²³ on surface of a scintillator bar, as shown in the Fig 11. 32 fibers are gathered together by
¹²⁴ a fiber bundle at edge of the module, and lead scintillation light to a 32-channel arrayed

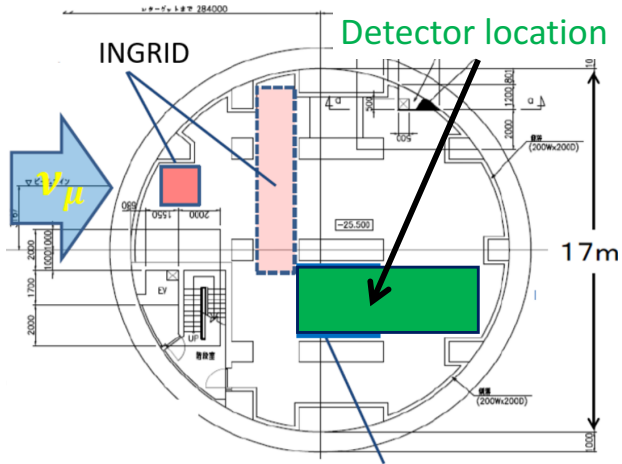


Figure 3: Candidate detector position in the B2 floor of the near detector hall.

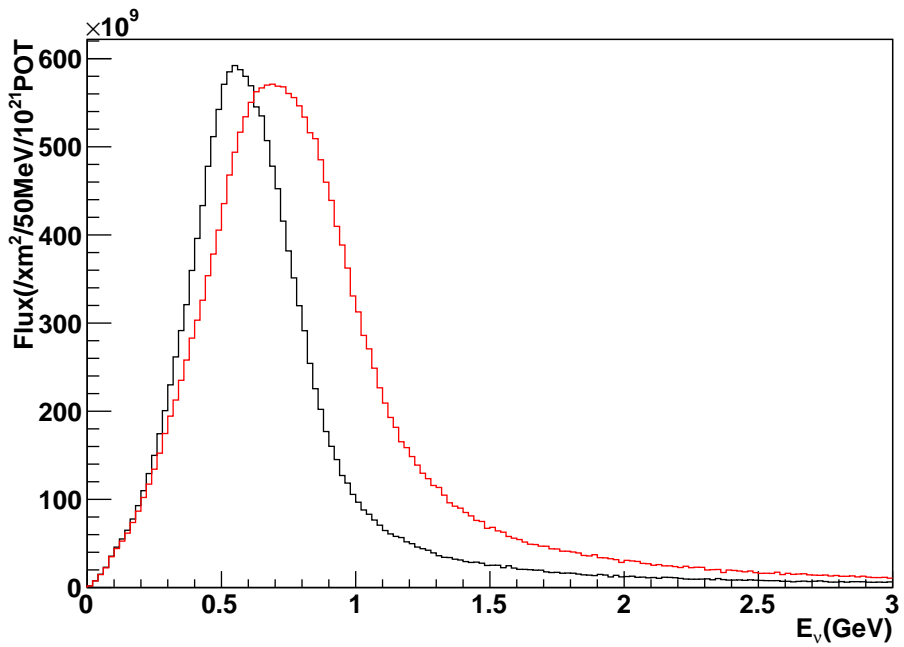


Figure 4: Neutrino energy spectrum at the candidate detector position(red, off-axis 1.5 degree). The spectrum at the ND280 site (black, off-axis 2.5 degree) is also shown.

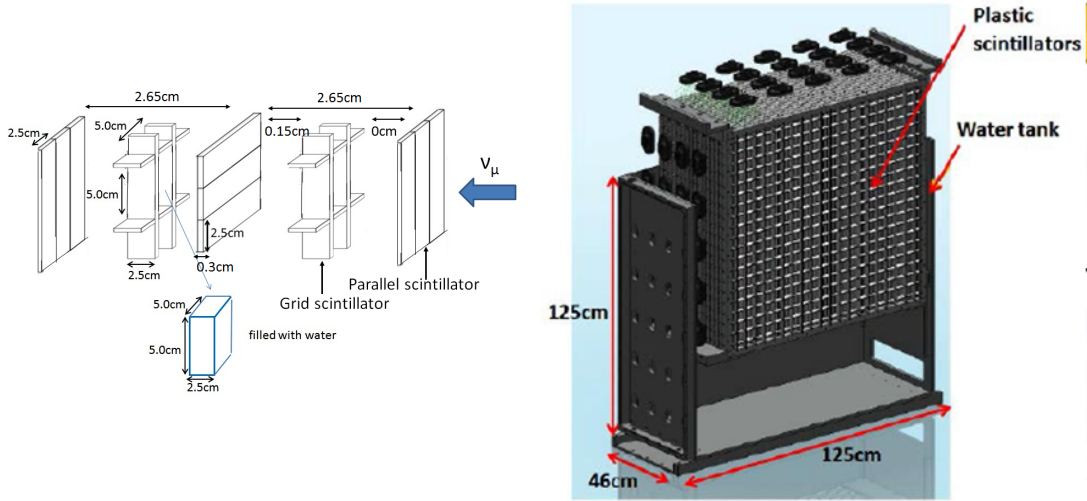


Figure 5: Schematic views of 3D grid-like structure of plastic scintillator bars (left) and Wagasci module (right).

MPPC. Since crosstalk of light yield due to reflection on the inner surface of each cell has been observed, all the scintillator bars are painted black by aqueous color spray, as shown in Fig 12. It is confirmed by measurements with cosmic rays that black painting on the surface of the scintillator bars suppresses this crosstalk so that no significant crosstalk effect is observed within uncertainty.

32-channel arrayed MPPCs, as shown in the Fig 13, are used for this module. The surface of the fiber bundle is polished and directly attached onto the 32-channel arrayed MPPCs. The positions of 32 fibers on the bundle are aligned to fit the channels of MPPCs. The MPPC is a product of Hamamatsu Photonics, S13660(ES1), with suppressed noise rate of ~ 6 kHz per channel at 0.5 p.e. For each MPPC channel 716 pixels of APD are aligned in a shape of circle.

2.1.2 Electronics

As front-end electronics of this detector, a Silicon PM Integrated Read-Out Chip (SPIROC) [3] is adopted. SPIROC is a 36-channel auto-triggered front-end ASIC, and is produced by OMEGA/ IN2P3. It not only contains an analog signal processing part such as amplification and shaping of the waveform, but contains a digital signal processing parts such as auto-trigger and timing measurement. Charge of MPPC signal is sampled by track-and-hold circuit. A Front-end electronics board, Active Sensor Unit (ASU), has been developed with the SPIROC2D chip, which is the latest version of SPIROC. Each readout board is

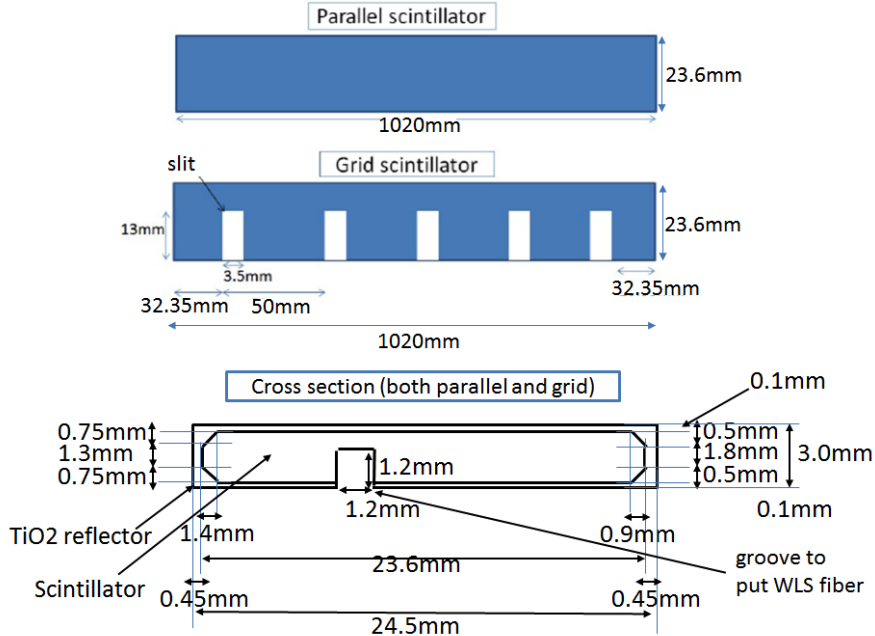


Figure 6: Geometry of scintillators used for Wagasci modules.

144 designed to control a 32-channel arrayed MPPC, and 40 of the ASU boards are aligned
 145 on the module surface as shown in Fig 14. The data acquisition system used for this
 146 detector, including back-end boards, has been developed for prototypes of ultra-granular
 147 calorimeters for the International Linear Collider (ILC) [2], and independent of the T2K
 148 DAQ system. To synchronize the DAQ system to J- PARC neutrino beam, pre-beam
 149 trigger and beam trigger are sent to the clock control card. The beam trigger signals are
 150 converted from optical signals to NIM signals at NIM module on the B2 floor. In addition,
 151 the information of spill number are delivered with 16-bit ECL level signals, and converted
 152 to an Ethernet frame by an FPGA evaluation board to be directly sent to the DAQ PC.

153 **2.1.3 Water system**

154 **2.2 INGRID Proton module**

155 INGRID Proton module is a neutrino detectors of the T2K experiment. It is a fully-active
 156 tracking detector which consists of only scintillator strips. The purpose of this Proton
 157 Module is to separate the neutrino interaction types by detecting the protons and pions
 158 together with the muons from the neutrino interactions, and to measure the neutrino cross
 159 section for each interaction type. It consists of 36 tracking planes surrounded by veto planes

(Figure ??), where each tracking plane is an array of two types of scintillator strips. The 16 strips in the inner region have dimensions of $2.5\text{cm} \times 1.3\text{cm} \times 120\text{cm}$, while the 16 strips in the outer region have dimensions of $5\text{cm} \times 1\text{cm} \times 120\text{cm}$, making a plane of $120 \times 120\text{cm}^2$ in the horizontal and vertical directions. The former is the scintillator produced for the K2K SciBar detector [?] and the latter was produced for INGRID. The tracking planes are placed perpendicular to the beam axis at 23mm intervals. Since the strips are aligned in one direction, each tracking plane is sensitive to either the horizontal or vertical position of the tracks. The tracking planes are therefore placed alternating in the horizontal and vertical directions so that three-dimensional tracks can be reconstructed. The tracking planes also serve as the neutrino interaction target. As with the Wagasci modules, scintillation light is read out by a WLS fiber and MPPC.

It was installed at the neutrino beam axis on the SS floor of the T2K near detector hall in 2010, and had been used for neutrino cross section measurements. In August 2017, it was moved to the B2 floor of the T2K near detector hall by J-PARC T59 after getting the approval from T2K to use them. J-PARC T59 is performing a neutrino beam measurement using the detector from October 2017, and the measurement will continue until May 2018 as we will discuss in Sec. ??.



Figure 7: Schematic view of INGRID Proton module.

177 **2.3 Baby MIND**

178 The Baby MIND is the downstream Muon Range Detector. It also works as a magnet and
179 provides the charge identification capability as well as magnetic momentum measurement
180 for high energy muons.

181 The Baby MIND collaboration ¹ submitted a proposal to the SPSC at CERN, SPSC-P-
182 353. The project was approved by the CERN research board as Neutrino Platform project
183 NP05 and constructed. The detector consists of 33 magnet modules, each 3500 mm ×
184 2000 mm × 50 mm (30 mm steel) with a mass of approximately 2 tonnes. Of these magnet
185 modules, 18 are instrumented with plastic scintillator modules.

186 **2.3.1 Magnet modules**

187 The Baby MIND is built from sheets of iron interleaved with scintillator detector modules
188 but unlike traditional layouts for magnetized iron neutrino detectors (e.g. MINOS) which
189 tend to be monolithic blocks with a unique pitch between consecutive steel segments and
190 large conductor coils threaded around the whole magnet volume, the Baby MIND iron
191 segments are all individually magnetized as shown in Fig. ??, allowing for far greater
192 flexibility in the setting of the pitch between segments, and in the allowable geometries
193 that these detectors can take.

194 The key design outcome is a highly optimized magnetic field map. A double-slit configura-
195 tion for coil winding was adopted to increase the area over which the magnetic flux
196 lines are homogeneous in B_x across the central tracking region. Simulations show the
197 magnet field map to be very uniform over this central tracking region covering an area of
198 2800×2000 mm², Fig. ?? . The B_x component dominates in this region, with negligible
199 B_y and B_z . This was confirmed by measuring the field with 9 pick-up coils wound around
200 the first module. Subsequent modules were equipped with one pick-up coil. Test results
201 on the 33 modules show all to achieve the required field of 1.5 T for a current of 140 A,
202 with a total power consumption of 11.5 kW. The polarity of the field map shown in Fig. ??
203 (middle) can be reversed by changing the power supply configuration.

204 **2.3.2 Scintillator modules**

205 Each of the 18 scintillator modules is constructed from 2 planes of horizontal counters (95
206 counters in total) and 2 planes of vertical counters (16 counters in total) [?], arranged
207 with an overlap between planes to achieve close to 100% hit efficiency for minimum ioniz-
208 ing muons. The arrangement of planes within a module is vertical-horizontal-horizontal-
209 vertical. This arrangement was the result of an assembly approach whereby each plane
210 was built from 2 half-planes, with each half plane consisting of a horizontal plane and a
211 vertical plane. The scintillator bars are held in place using structural ladders that align

¹Contact person: E. Noah, Spokesperson: A. Blondel, Deputy spokesperson: Y. Kudenko

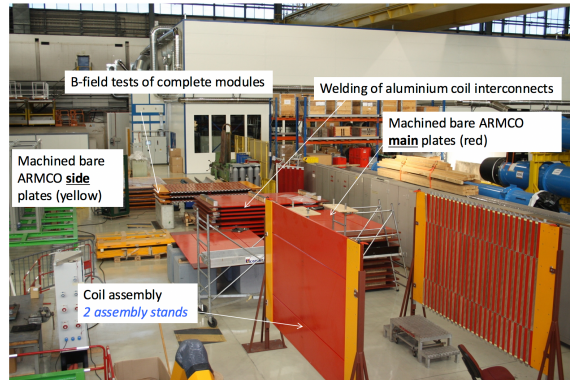


Figure 8: Magnet assembly zone at CERN.

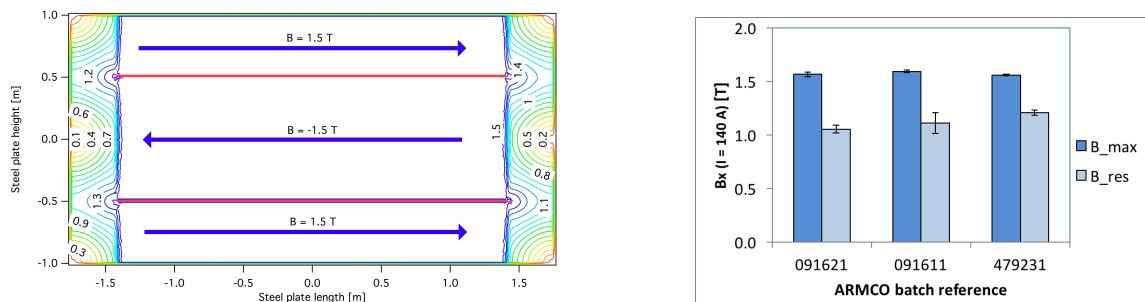


Figure 9: Left) Magnetic field map with a coil along 280 cm of the length of the plate. Right) Measured B field for 33 modules.

212 and maintain the counters, Fig. ???. No glue is used in the process, so counters can be
213 replaced. Aluminum sheets front and back provide light tightness.



Figure 10: Scintillator modules assembly. Left) top of front half-module showing vertical counters and the spacers-ladders that set the pitch between horizontal counters and hold them in place. Middle) rear half-module showing horizontal counters on their ladders. Right) Assembled rear half-module, the front half-module can be seen in the background.

214 The plastic scintillator counters were made from 220 mm-wide slabs, consisting of
215 extruded polystyrene doped with 1.5% paraterphenyl (PTP) and 0.01% POPOP. They were
216 cut to size then covered with a 30-100 μm thick diffuse reflector resulting from etching of
217 the surface with a chemical agent [?, ?]. The horizontal counter size is $2880 \times 31 \times 7.5 \text{ mm}^3$,
218 with one groove along the length of the bar in which sits a wavelength shifting fiber from
219 Kuraray. The vertical counter size is $1950 \times 210 \times 7.5 \text{ mm}^3$, with one U-shaped groove
220 along the bar. On each counter, two custom connectors house silicon photomultipliers,
221 MPPC type S12571-025C from Hamamatsu, either side of the horizontal counter, and
222 both connectors at the top for the vertical counter. This geometrical configuration for
223 vertical counters was chosen for ease of connectivity to the electronics, and maintenance
224 operations.

225 A total of 1744 horizontal counters and 315 vertical counters (including spares) were
226 produced at the Uniplast company (Vladimir, Russia).

227 **2.3.3 Electronics**

228 The Baby MIND electronic readout scheme includes several custom-designed boards [?].
229 The revised version is shown in Fig. ???. At the heart of the system is the electronics
230 Front End Board (FEB), developed by the University of Geneva. The readout system
231 includes two ancillary boards, the Backplane, and the Master Clock Board (MCB) whose
232 development has been managed by INRNE (Bulgarian Academy of Sciences) collaborators.

233 The FEBv2 hosts 3 CITIROC chips that can each read in signals from 32 SiPMs [?].
234 Each signal input is processed by a high gain, and a separate low gain, signal path. The
235 outputs from the slow shapers can be sampled using one of two modes: a mode with an
236 externally applied delay, and a peak detector mode. A faster shaper can be switched to
237 either HG or LG paths, followed by discriminators with adjustable thresholds providing 32

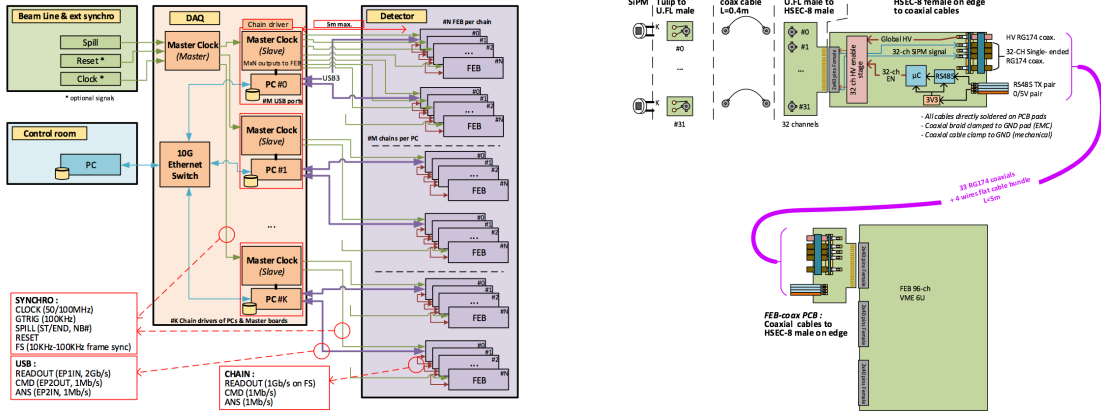


Figure 11: Left) Baby MIND electronics readout scheme. Right) SiPM-to-FEB connectivity.

individual trigger outputs and one OR32 trigger output. An Altera ARIA5 FPGA on the FEBv2 samples these trigger outputs at 400 MHz, recording rising and falling times for the individual triggers and assigning time stamps to these. Time-over-threshold from the difference between falling and rising times gives some measure of signal amplitude, used in addition to charge information and useful if there is more than one hit per bar within the deadtime due to the readout of the multiplexed charge output of $\sim 9 \mu\text{s}$. The ARIA5 also manages the digitization of the sampled CITIROC multiplexed HG and LG outputs via a 12-bit 8-ch ADC.

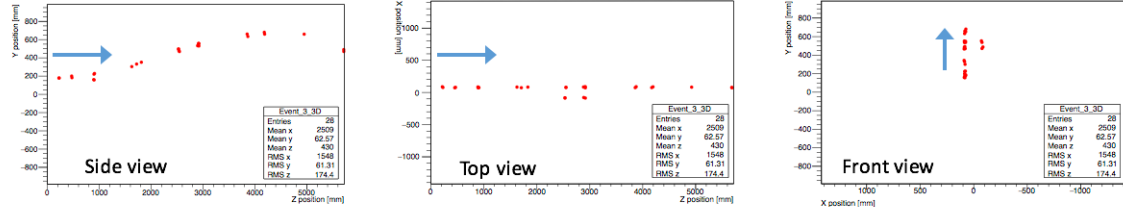
The internal 400 MHz clock on the FEBv2 can be synchronized to a common 100 MHz clock. The synchronization subsystem combines input signals from the beam line into a digital synchronization signal (SYNC) and produces a common detector clock (CLK) which can eventually be synchronised to an external experiment clock. Both SYNC and CLK signals are distributed to the FEBs. Tests show the FEB-to-FEB CLK(SYNC) delay difference to be 50 ps (70 ps). Signals from the beam line at WAGASCI include two separate timing signals, arriving 100 ms and 30 μs before the neutrino beam at the near detectors. The spill number is available as a 16-bit signal.

2.3.4 Pefromance check

All counters were measured at INR Moscow with a cosmic ray setup using the same type S12571-025C MPPCs and CAEN DT5742 digitizer. The average light yield (sum from both ends) was measured to be 37.5 photo-electrons (p.e.) per minimum ionizing particle (MIP) and 65 p.e./MIP for vertical and horizontal counters, respectively. After shipment to CERN, all counters were tested once more individually with an LED test setup [?]. 0.1% of counters failed the LED tests and were therefore not used during the assembly of modules.

261 The assembly of modules was completed in June 2017, and it was then tested in June and
 262 July 2017 at the Proton Synchrotron experimental hall at CERN with a mixed particle
 263 beam comprising mostly muons whose momenta could be selected between 0.5 and 5 GeV/c.
 An event display from the summer 2017 tests is shown in Fig. ??.

Beam Muon 2 GeV/c



Cosmic Muon

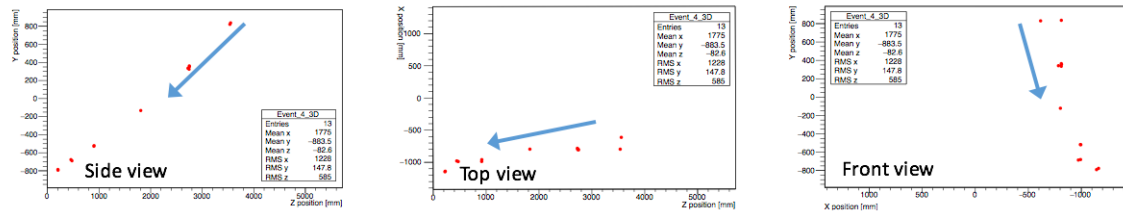


Figure 12: Comparison of a beam muon and cosmic muon in the three different geometrical projections of the detector. The beam impinges on the detector from the left. The arrows indicate the direction of travel of these muons. The direction of the cosmic muon is inferred from timing information.

264

2.4 Side muon range detector

265 Two Side-MRD modules for tracking secondary particles from neutrino interactions will be
 266 installed in 2018. Each Side-MRD module is composed of 11 steel plates and 10 layers of
 267 total 80 scintillator slabs installed in 13 mm gaps between the 30 mm thick plates. Each
 268 steel plate size is $30 \times 1610 \times 1800$ mm 3 . Total module size is $2236 \times 1630 \times 975$ mm 3 as
 269 shown in Fig. ?? (left), weight is ~ 8.5 ton.

270 Scintillator bars were manufactured by Uniplast company in Vladimir, Russia. Polystyrene
 271 based scintillators were extruded with thickness of 7 mm, then cut to the size of $7 \times 200 \times$
 272 1800 mm 3 . Dopant composition is 1.5% PTP and 0.01% POPOP. Scintillator surface was
 273 etched by a chemical agent to form a white diffuse layer with excellent reflective perfor-
 274 mance. Ideal contact between the scintillator and the reflector raises the light yield up to
 275 50% comparing to an uncovered scintillator. Sine like groove was milled along the scin-
 276 tillator to provide uniform light collection over the whole scintillator surface. WLS Y11
 277 Kuraray fiber of 1 mm diameter is glued with an optical cement EJ-500 in the S-shape

279 groove as shown in Fig. ??(right). Bending radius is fixed to 30 mm that was specified to
 280 be safe for Kuraray S-type fibers. Both ends of the fiber are glued into optical connectors
 281 which mounted within a scintillator body and provide an interface to SiPMs, Hamamatsu
 282 MPPC S13081-050CS(X1).

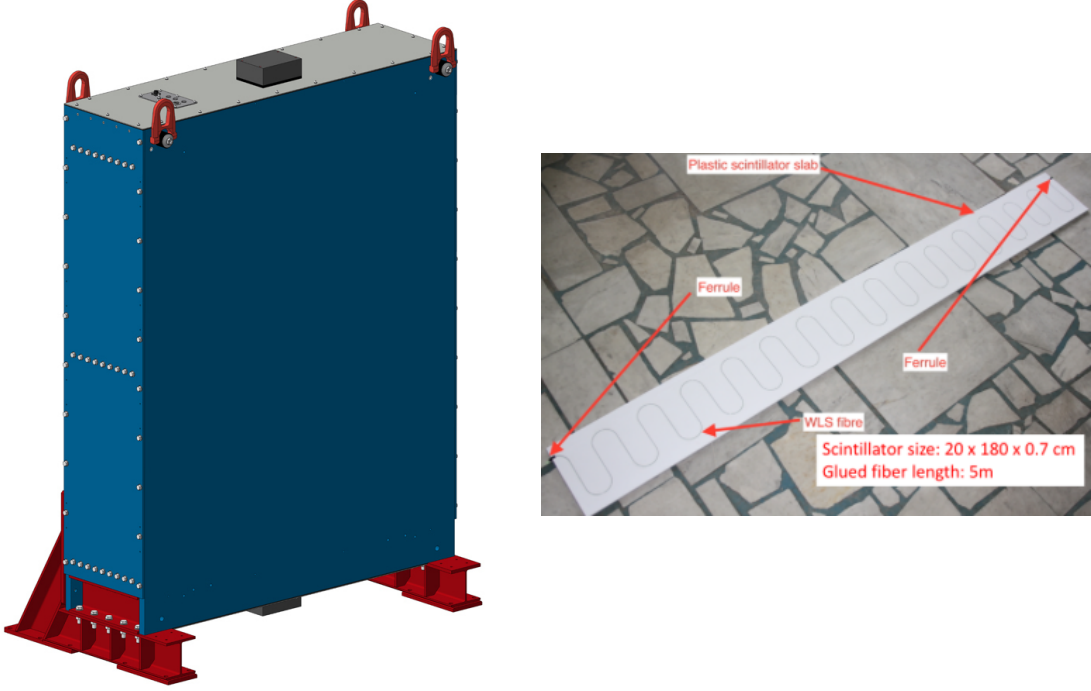


Figure 13: Left :Side-MRD module. Right: Scintillator bar of the Side-MRD modules.

283 Scintillators for the Side-MRD modules had been assembled at INR in Russia, and
 284 shipped to Japan in July 2017. The light yield for each scintillator was measured with
 285 cosmic rays at INR and at YNU in Japan after delivery. Parameters measured at the
 286 center of the counter were : the light yields LY_1 and LY_2 at both ends, the light yield
 287 asymmetry between the ends calculated as $100\% \times \frac{LY_1 - LY_2}{LY_1 + LY_2}$. After tests at INR we selected
 288 324 counters from measured 332 ones with the mean light yield of 45 p.e./MIP ($LY_1 + LY_2$)
 289 and the asymmetry value less than 10 %. The measuremens at YNU yielded the average
 290 total light yield of about 40 p.e./MIP which varies in range from 32 to 50 p.e./MIP (Fig.
 291 ?? (left)). Only two counters showed relatively high asymmetry close to 25 % as shown in
 292 Fig. ?? (right). Using the results of the quality assurance test we selected 320 scintillator
 293 counters for the Side-MRD modules.

294 We also measured the time resolution for a combination of four counters piled each on

295 another one. The average result for four counters is $\sigma_T = 1.04$ ns. The resolution of com-
 296 bination of 2, 3, 4 counters is measured to be 0.79 ns, 0.66 ns and 0.58 ns, correspondently.

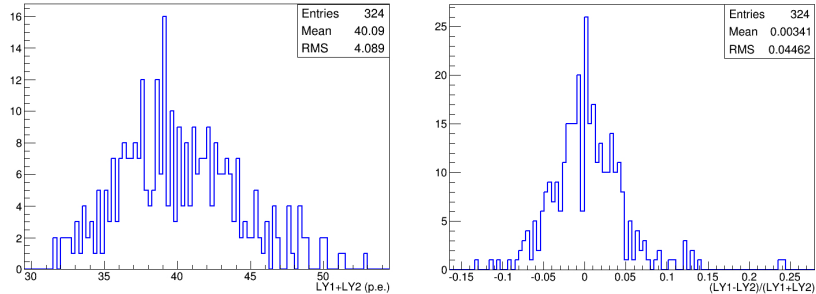


Figure 14: Total light yield distribution (left) and light yield assymetry (right) measured at YNU.

297
 298 Construction of Side-MRD modules will be done from November 2017 at Yokohama
 299 National University, then they will be transported to J-PARC and will be installed at B2
 300 floor of the T2K near detector hall.

301 3 Physics goals

302 We will measure the differential cross section for the charged current interaction on H_2O
 303 and Hydrocarbon(CH)). The water-scintillator mass ratio of the Wagasci module is as
 304 high as 5:1 and the high purity measurement of the cross section on H_2O is possible. One
 305 experimental option is to remove water from one of the two Wagasci modules. The water-
 306 out WAGASCI module will allow to measure pure-CH target interactions with very low
 307 momentum-threshold for protons. It will also benefit to subtract the background from
 308 interaction with scintillator in the water target measurement. Another option is to add
 309 the T2K proton module which is fully made of plastic scintillators. It will allow the high
 310 statistics comparison of cross section between H_2O and CH and also comparison with
 311 the ND280 measurement. The actual configuration will be optimized with detailed MC
 312 simulation by 2018 Summer.

313 Our setup allows the measurements of inclusive and also exclusive channels such as $1-\mu$,
 314 $1-\mu 1p$, $1-\mu 1\pi \pm np$ samples, former two of which are mainly caused by the quasi-elastic and
 315 2p2h interaction and the latter is mainly caused by resonant or coherent pion production
 316 and deep elastic scattering. In general, an accelerator produced neutrino beam spectrum
 317 is wide and the energy reconstruction somehow rely on the neutrino interaction model.
 318 Therefore, recent neutrino cross section measurement results including those from T2K

319 are given as a flux-integrated cross section rather than cross sections as a function of
320 the neutrino energy to avoid the model dependency. We can provide the flux-averaged
321 cross section. In addition, by combining our measurements with those at ND280, model-
322 independent extraction of the cross section for narrow energy region becomes possible.
323 This method was demonstrated in [?] and also proposed by P** (NUPRISM).

324 **3.1 Expected number of events**

325 Expected number of neutrino events after the event selections is evaluated with Monte Carlo
326 simulations as we will discuss in Section ???. In the neutrino-mode, 4.2×10^3 , 1.1×10^3
327 and 3.8×10^3 CC neutrino events are expected in the water-in WAGASCI module, the
328 water-out WAGASCI module and the INGRID proton module after the selections with
329 0.5×10^{21} POT, and its purities are 78.0 %, 97.5 % and $\sim 98\%$. In the antineutrino-mode,
330 1.7×10^3 , 0.4×10^3 and 1.5×10^3 CC antineutrino events are expected in the water-in
331 WAGASCI module, the water-out WAGASCI module and the INGRID proton module
332 after the selections with 0.5×10^{21} POT, and its purities are 59.5 %, 74.4 % and $\sim 74\%$.

333 Statical errors of flux integrated CC-inclusive neutrino cross section measurements on
334 H₂O (full acceptance) and CH targets (forward acceptance) will be 1.5 % and 1.6 % with
335 0.5×10^{21} POT in the neutrino-mode. Statical errors of flux integrated CC-inclusive anti-
336 neutrino cross section measurements on H₂O (full acceptance) and CH targets (forward
337 acceptance) will be 2.4 % and 2.5 % with 0.5×10^{21} POT in the antineutrino-mode.

338 Statical errors of flux integrated H₂O to CH CC-inclusive neutrino cross section ratio
339 measurement will be 3.1 % (full acceptance) and 2.3 % (forward acceptance) with 0.5×10^{21}
340 POT in the neutrino-mode. Statical errors of flux integrated H₂O to CH CC-inclusive
341 antineutrino cross section ratio measurement will be 5 % (full acceptance) and 3.7 %
342 (forward acceptance) with 0.5×10^{21} POT in the antineutrino-mode.

343 **3.2 Pseudo-monochromatic beam by using different off-axis fluxes**

344 The off-axis method gives narrower neutrino spectrum, and the peak energy is lower for
345 larger off-axis angle. There still remains high energy tail mainly due to neutrinos from
346 Kaon decay. The off-axis angle of the Wagasci location is 1.5 degree and different from the
347 ND280 2.5 degree. Top two plots of Fig. ?? show the energy spectra of fluxes and neutrino
348 interaction events at these two different location. The high energy tail of ND280 flux can
349 be somehow subtraction by using the Wagasci measurement. The low energy part of the
350 Wagasci flux can be also subtracted by using the ND280 measurement. Bottom two plots
351 of Fig. ?? demonstrate this method. We can effectively get two fluxes, from 0.2 GeV to
352 0.9 GeV and 0.6 GeV and 2 GeV and measure flux-integrated cross section for these two
353 fluxes.

354 Statical errors of flux integrated CC-inclusive neutrino cross section measurements
355 on H₂O (forward acceptance) and CH targets (forward acceptance) with the pseudo-

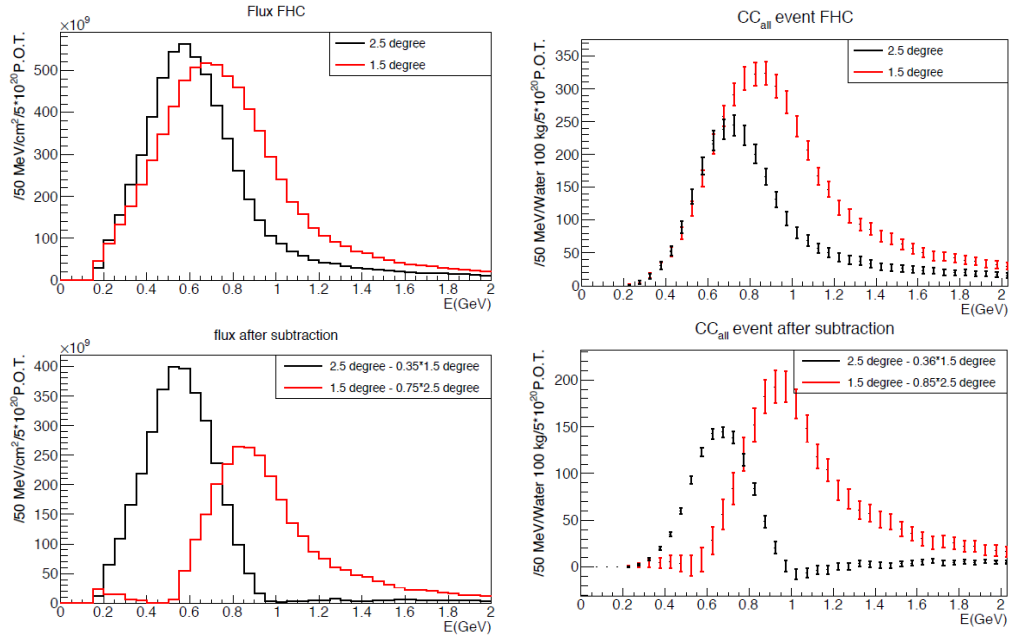


Figure 15: Energy spectra obtained by using different off-axis angle fluxes. Top two plots show the fluxes(left) and spectra of interaction events (right) for ND280 (off-axis 2.5 degree) and Wagasci (off-axis 1.5 degree). Bottom two plots show the fluxes (left) and spectra of interaction events (right) obtained by subtraction of fluxes at ND280 and Wagasci. The error bar is for the statistical error and those in the bottom right plot is obtained assuming the statistical error for ND280 measurement is much smaller than that of Wagasci experiment.

monochromatic beam will be 2 % and 1.9 % with 0.5×10^{21} POT in the neutrino-mode. Statical errors of flux integrated CC-inclusive antineutrino cross section measurements on H₂O (forward acceptance) and CH targets (forward acceptance) with the pseudo-monochromatic beam will be 3 % and 2.8 % with 0.5×10^{21} POT in the neutrino-mode.

3.3 Subjects Wagasci can contribute

In T2K experiment, neutrinos interact with bound nucleons in relatively heavy nuclei (Carbon and Oxygen), so the cross-section is largely affected by nuclear effects. The nuclear effects are categorized as nucleons' momentum distribution in nucleus, interactions with correlated pairs of nucleons in nucleus (two particles-two holes, 2p2h), collective nuclear effects calculated with Random Phase Approximation (RPA) and final state interactions (FSI) of secondary particles in the nuclei after the initial neutrino interactions.

367 The 2p2h interactions mainly happen through Δ resonance interactions following a
 368 pion-less decay and interactions with a correlated nucleon pair. The 2p2h interactions are
 369 observed in electron scattering experiments [?] where the 2p2h events observed in the gap
 370 between Quasi-Elastic region and Pion-production region as shown in Fig. ???. Neutrino
 371 experiments also attempt to measure the 2p2h interactions, but separation of the QE peak
 372 and the 2p2h peak is more difficult because transferred momentum (p) and energy (w)
 373 are largely affected by neutrino energies which cannot be determined event-by-event in the
 374 wide energy spectrum of the accelerator neutrino beam. Our model-independent narrow
 375 neutrino spectra extracted from combined analyses of our data and ND280 data are ideal
 376 for searching the 2p2h interaction because clearer separation of the QE peak and the 2p2h
 377 peak is expected. Another way to observe the 2p2h interaction is direct measurement of
 378 proton tracks in CC0 π sample with low detection threshold and full acceptance. Fig. ??
 379 shows proton multiplicities after FSI in CCQE events and 2p2h events, and Fig. ?? shows
 380 opening angles among two proton tracks in the same samples. The water-out Wagasci
 381 can provide good sample for the 2p2h interaction search because its low density medium
 382 enables the detection of low momentum protons in addition to the full acceptance.

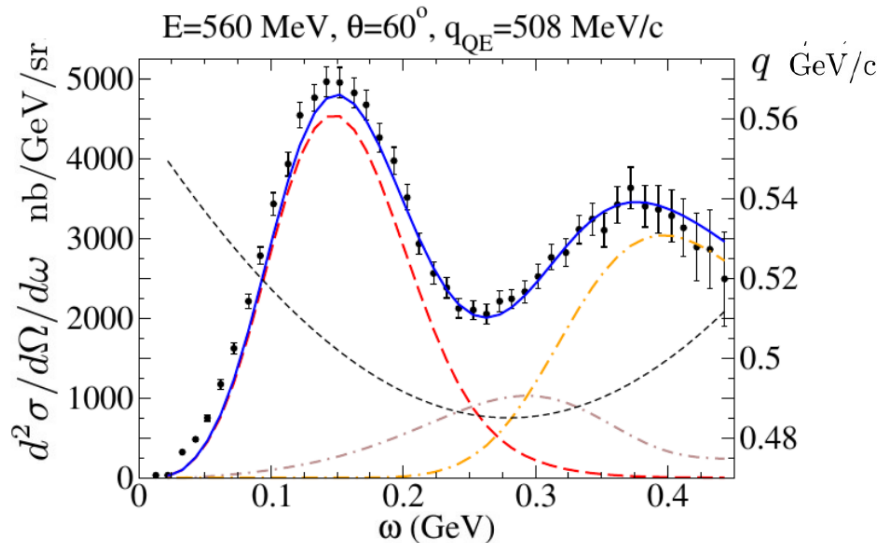


Figure 16: Comparison of inclusive $^{12}\text{C}(\text{e},\text{e}')$ cross sections and predictions of the QE-SuSAv2 model (long-dashed red line), 2p-2h MEC model (dot-dashed brown line) and inelastic-SuSAv2 model (long dot-dashed orange line) (from Ref. [?]). The sum of the three contributions is represented with a solid blue line. The q dependence with w is also shown (short-dashed black line.)

383 The corrections from collective nuclear effects calculated by RPA as a function of Q^2 are

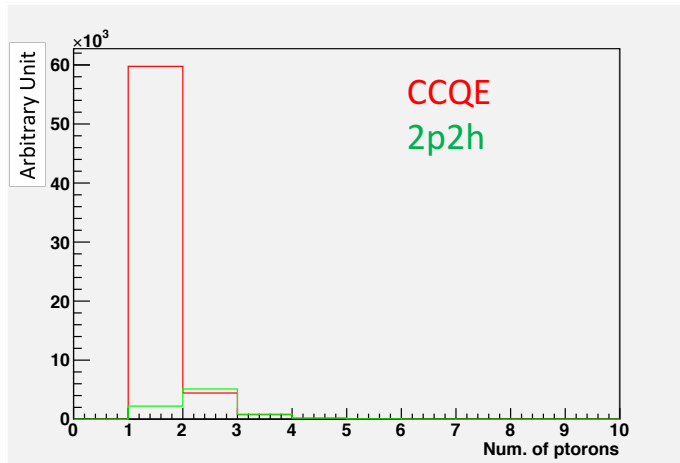


Figure 17: Proton multiplicities after FSI in CCQE events and 2p2h events.

384 shown in Fig. ???. The Q^2 dependence of the correction can be tested by measuring angular
 385 distribution of muons in CC1- μ and CC1- $\mu 1p$ events. The uncertainties of the corrections
 386 in low (high) Q^2 regions can be constrained by observing the events with a forward-going
 387 (high-angle) muon, so it is essential to measure muon tracks with full acceptance.

388 T2K experiment is starting to use ν_e CC1 π events for its CP violation search to increase
 389 the statistics. One of the biggest uncertainty of the CC1 π sample comes from the final
 390 state interactions of pions in the nuclei after the initial neutrino interactions because they
 391 change the multiplicity, charge and kinematics of the pions. The multi-pion production
 392 events can be migrated into the CC1 π sample due to the FSIs, and they become important
 393 backgrounds. We can constrain the uncertainties from the pion FSIs by measuring pion
 394 rescattering in the detector and pion multiplicity in ν_μ CCn π sample with low detection
 395 threshold and full acceptance for pion tracks. The water-out WAGASCI can provide good
 396 sample for the pion FSI studies because its low density medium enables the detection of
 397 low momentum pions in addition to the full acceptance.

398 4 Status of J-PARC T59 experiment

399 We had submitted a proposal of a test experiment to J-PARC in April 2014 to test a new
 400 detector with a water target, WAGASCI, at the neutrino monitor hall, and the proposal
 401 was approved as J-PARC T59. The project contains the side and downstream muon range
 402 detectors as well.

403 The first WAGASCI module has been constructed in 2016 and installed at the on-

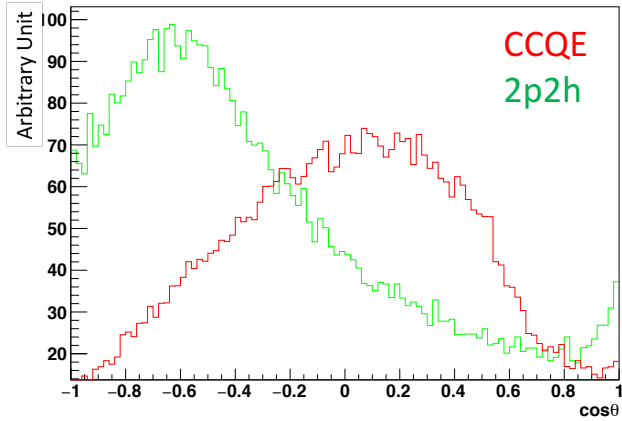


Figure 18: Opening angles among two proton tracks after FSI in CCQE events and 2p2h events.

axis position in front of the T2K INGRID detector for the commissioning and the first cross section measurement as a part of the T2K experiment. The INGRID electronics boards are used to read the signal. The light yield measured with muons produced by the interaction of neutrinos in the hall wall, shown in Fig. ??, is sufficiently high to get good hit efficiency. A track search algorithm based on the cellular automaton has been developed using the software tools by the T2K INGRID. Examples of observed events are shown in Fig. ?? The tracking efficiency in 2-dimensional projected plane was evaluated by comparing the reconstructed track in the WAGASCI module and the INGRID module and shown in Fig. ?? Note that that the tracking efficiency for high angle (> 70 deg) is not evaluated because of the acceptance of the INGRID module, not because of the limitation of the WAGASCI module.

In 2017 Autumn, the construction of the second WAGASCI module and the dedicated electronics board were completed. The module and the electronics were install to the B2 floor together with the T2K proton module and the INGRID module as shown in Fig. ?? The proton module is to be used as the entering muon veto and also for the comparison of interaction between CH and Water. The INGRID module is for the temporary muon detector with limited acceptance for this period. The detector was commissioned and is in operation to take data with the antineutrino beam during the T2K beam time from October.

The production of the components of the side muon range detectors has been completed and now the detectors are being assembled at the Yokohama National University. These

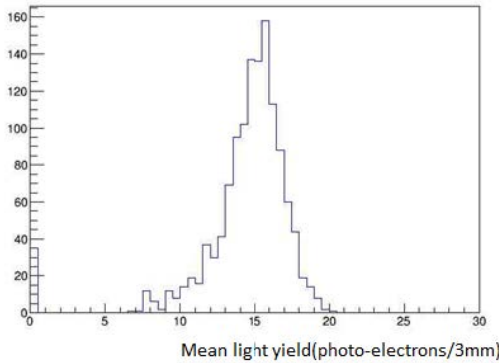


Figure 19: Light yield for muons produced by the interaction of neutrinos in the hall wall. Average light yields for each channel are plotted.

425 detectors will be installed sometime from January to June, 2018 when T2K is not running.
 426 The Baby MIND detector was transported from CERN to Japan in December, 2017.
 427 It will be installed and commissioned in Jan.-Feb. 2018 and T59 will take the neutrino-
 428 induced muon data in April and May.

429 5 MC studies

430 5.1 Detector simulation

431 Expected number of neutrino events in the water-in Wagasci detector is evaluated with
 432 Monte Carlo simulations. Neutrino beam flux at the detector location is simulated by
 433 T2K neutrino flux generator, JNUBEAM, neutrino interactions with target materials are
 434 simulated by a neutrino interaction simulator, NEUT, detector responses are simulated
 435 using GEANT4-based simulation. The neutrino flux at the detector location, 1.5 degrees
 436 away from the J-PARC neutrino beam axis, is shown in Figure ??, and its mean neutrino
 437 energy is around 0.68 GeV.

438 5.1.1 Detector geometry

439 The detector geometry in the GEANT4-based simulation is slightly different from the actual
 440 detector as shown in Fig. ???. The active neutrino target region consists of four Wagasci
 441 modules, and each Wagasci detector has the dimension with 100 cm \times 100 cm in the x and
 442 y directions and 50 cm along the beam direction. Two Side-MRD modules is installed at
 443 both sides of the Wagasci modules, and each Side-MRD module consists of ten iron plates
 444 whose dimension is 3 cm (thickness) \times 200 cm (height) \times 320 cm (width). The distance

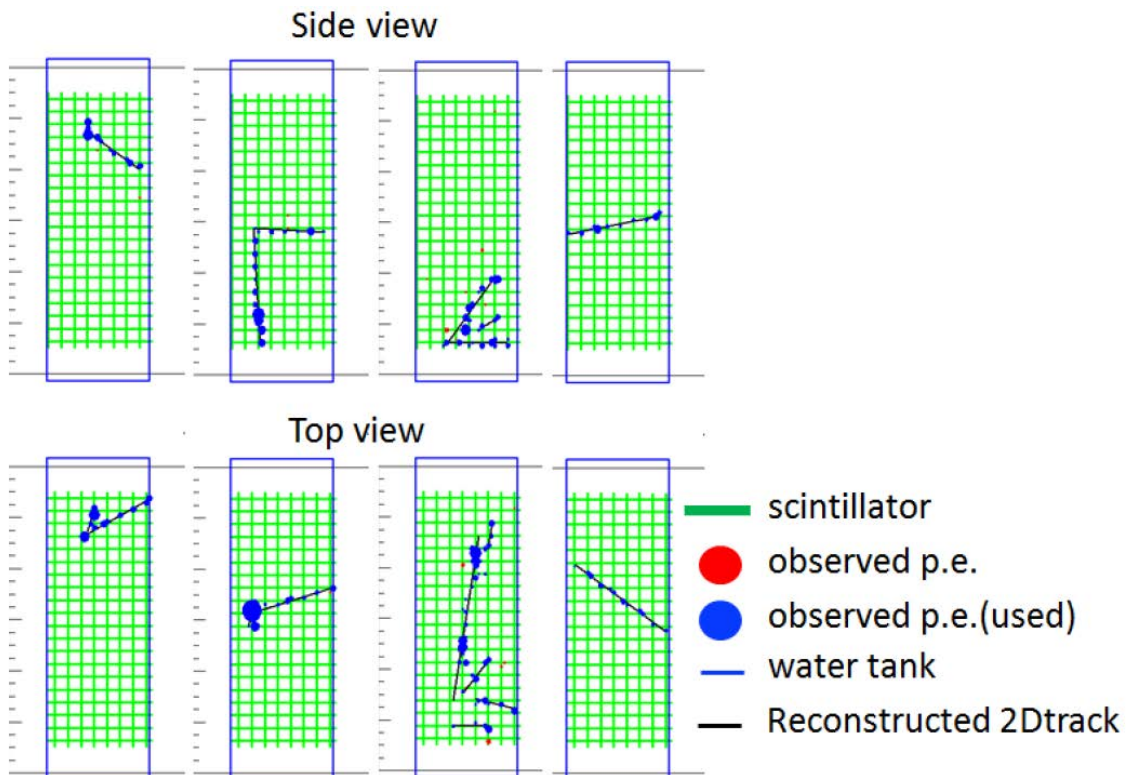


Figure 20: Example event displays of the WAGASCI module at on-axis. The reconstructed tracks are overlaid.

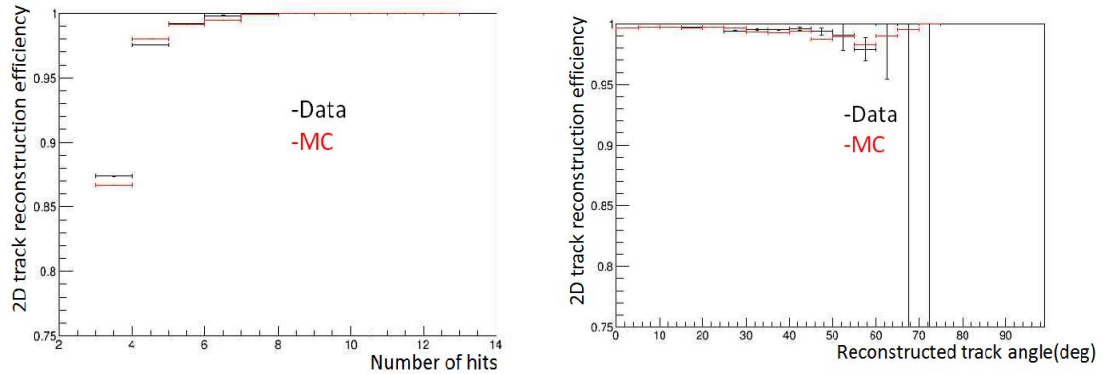


Figure 21: 2D track reconstruction efficiency as a function of number of hits (left) and track angle (right). Here the track angle is the one reconstructed by the INGRID module.

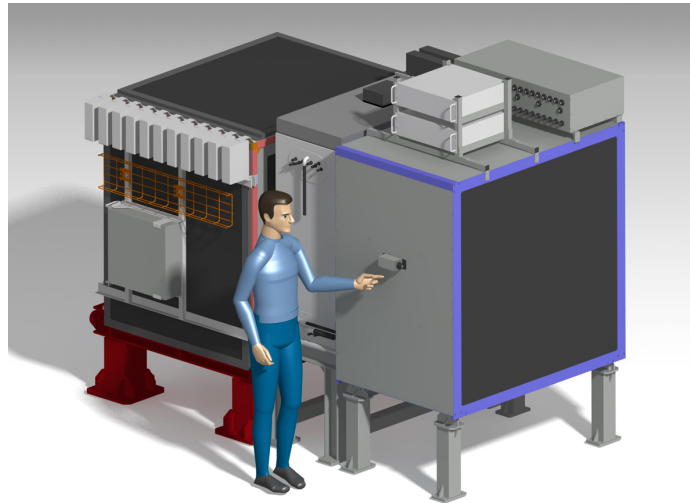


Figure 22: J-PARC T59 detector configuration in October 2017.

445 between the Side-MRD modules and Wagasci modules is 80 cm. The downstream-MRD
 446 equivalent to the Baby-MIND is installed at the downstream of the Wagasci modules. The
 447 downstream-MRD consists of thirty iron plates whose dimension is 3 cm (thickness) \times 200
 448 cm (height) \times 400 cm (width). The distance between the downstream-MRD modules and
 449 Wagasci modules is 80 cm.

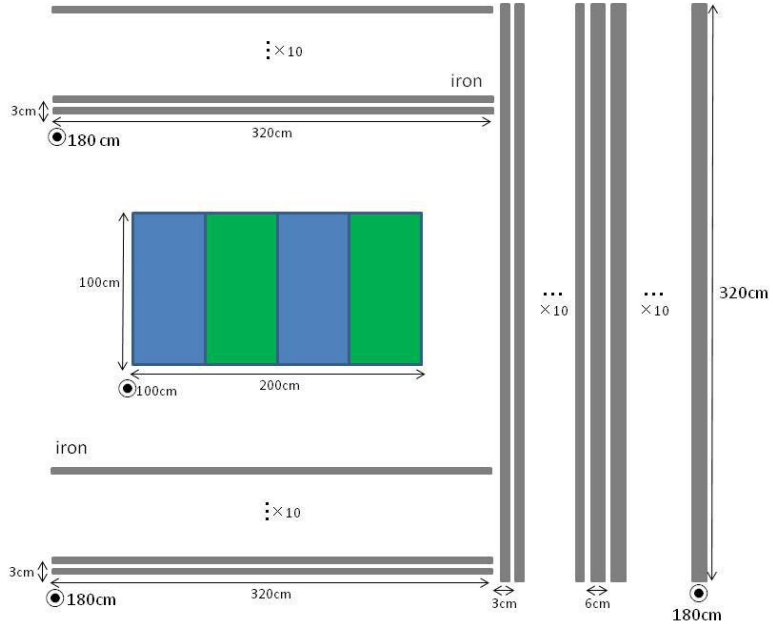


Figure 23: Geometry of the detectors in the Monte Carlo simulation.

450 5.1.2 Response of detector components

451 The energy deposit inside the scintillator is converted into the number of photons. The
 452 effects of collection and attenuation of the light in the scintillator and the WLS fiber are
 453 simulated, and the MPPC response is also taken into account. The light yield is smeared
 454 according to statistical fluctuations and electrical noise.

455 5.2 Track reconstruction

456 To select neutrino interaction from the hit patterns, a track reconstruction algorithm is
 457 developed. The flow of the track reconstruction is as follows.

458 1. Two-dimensional track reconstruction in each sub-detectors

- 459 2. Track matching among the sub-detectors
- 460 3. Three -dimensional track reconstruction
- 461 Add explanation about two-dim reco, track matching and three-dim reco here.

462 **5.3 Event selection**

463 First, the events with the track which starts in 5 cm from the wall of the Wagasci module
 464 are rejected to remove the background from the outside.

465 Second, to reject backgrounds from NC and neutral particles, the longest tracks are
 466 required to penetrate more than one (five) iron plates in Side-MRD modules (Baby-MIND).
 467 Then, in order to measure muon momentum, the longest tracks are required to stop in
 468 MRDs (Side-MRD modules and Baby-MIND) or penetrate all iron plates.

469 Table ?? and ?? show numbers of the selected events in one water-in Wagasci module
 470 after each event selection in neutrino-mode and antineutrino-mode respectively. As for
 471 the neutrino-mode, 8478 CC events are expected with 1×10^{21} POT, and the purity is
 472 78.0 %. The main background for the neutrino-mode is the neutrino interactions in the
 473 scintillators inside the Wagasci detector. As for the antineutrino-mode, 3331 CC events
 474 are expected with 1×10^{21} POT, and the purity is 59.5 %. The main background for the
 475 antineutrino-mode is the wrong sign contamination from ν_μ events and the antineutrino
 476 interactions in the scintillators inside the Wagasci detector.

Table 1: Expected number of the neutrino-candidate events in one water-in Wagasci module
 with 1×10^{21} POT in neutrino-mode.

Cut	CC	NC	Scinti Bkg.	Total
Reconstructed	18093.2	699.7	4698.3	23491.2
FV	15150.8	588.4	3934.8	19673.9
Pene. iron	11264.3	237.3	2875.4	14377.0
Stop/Penetrate MRDs	8478.2	214.0	2173.1	10865.2
after all cuts	78.0 %	2.0 %	20.0 %	100 %

477 Table ?? and ?? show numbers of the charged-current events in the water-in Wagasci
 478 module after all event selection with a classification based on interactions at a vertex with
 479 1×10^{21} POT in neutrino-mode and antineutrino-mode respectively.

480 Table ?? and ?? show numbers of the charged-current events in one water-in Wagasci
 481 module after all event selection with a classification based on particles after final state
 482 interactions with 1×10^{21} POT in neutrino-mode and antineutrino-mode respectively.

483 Figure ?? and ?? show the reconstructed angles of the longest tracks in the selected
 484 events in the neutrino-mode and the anti-neutrino mode respectively. Figure ??, ?? ??

Table 2: Expected number of the antineutrino-candidate events in one water-in Wagasci module with 1×10^{21} POT in antineutrino-mode.

Cut	CC	NC	Scinti Bkg.	Wrong sign bkg	Total
Reconstructed	6499.7	107.3	2234.4	2330.8	11172.1
FV	5457.9	89.3	1873.5	1946.6	9367.1
Pene. iron	4172.3	30.8	1440.9	1560.6	7204.6
Stop/Penetrate MRDs	3331.5	28.5	1120.3	1121.2	5601.5
after all cuts	59.5 %	0.5 %	20.0 %	20.0 %	100 %

Table 3: Expected number of the charged-current events in the water-in Wagasci module after the event selections with 1×10^{21} POT in neutrino-mode with a classification based on interactions at a vertex.

CCQE	MEC	CCRes	CDDIS	Total
3716.3	747.0	2081.3	1132.3	7676.9
48.4 %	9.7 %	27.1 %	14.7 %	100 %

485 and ?? show the iron plane numbers in Side-MRD and Baby-MIND corresponding to the
 486 end points of the longest tracks in the selected events in the neutrino-mode and the anti-
 487 neutrino mode.

488 5.4 Cross section measurements on water

489 In the water target events, the background from interaction with scintillators has to be
 490 subtracted by using the measurement of the hydrocarbon target.

Table 4: Expected number of the charged-current events in the water-in Wagasci module after the event selections with 1×10^{21} POT in antineutrino-mode with a classification based on interactions at a vertex.

CCQE	MEC	CCRes	CDDIS	Total
2522.0	362.8	765.8	765.8	4416.4
hline 57.1 %	8.2 %	17.3 %	17.3 %	100 %

Table 5: Expected number of the charged-current events in one water-in Wagasci module after the event selections with 1×10^{21} POT in neutrino-mode with a classification based on particles after final state interactions.

CC0 π	CC1 π	CC2 π	CCn π	Total
5423.1	1684.3	242.9	701.1	8051.4
67.4 %	20.9 %	3.0 %	8.7 %	100 %

Table 6: Expected number of the charged-current events in one water-in Wagasci module after the event selections with 1×10^{21} POT in antineutrino-mode with a classification based on particles after final state interactions.

CC0 π	CC1 π	CC2 π	CCn π	Total
2529.3	520.0	37.9	96.0	3183.2
79.5 %	16.3 %	1.2 %	3.0 %	100 %

491 **5.4.1 Charged current cross section measurement**

492 **6 Standalone WAGASCI-module performances**

493 In the previous sections, the WAGASCI detector was studied using the Muon Range Detectors. In this section, the standalone abilities of WAGASCI module are presented. Using
494 the WAGASCI configuration presented in Section ??, we have evaluated that only 7% of
495 the muons will be stopped in one of the WAGASCI modules. THowerver, this proportion
496 increases to 53% for pions and 73% for protons produced by neutrino interactions at 1.5°
497 off-axis. Figure ?? shows the momentum distribution of these daughter particles as well as
498 for the sub-sample stopped in one of the WAGASCI modules. Therefore, the study of the
499 standalone abilities of the WAGASCI module in this section are dominantly motivated by:
500

- 501 • the accurate measurement of the neutrino interaction final states. Though most of the
502 muons will be reconstructed and identified in the MRDs, the hadronic particles will
503 predominantly stops in one WAGASCI module. One has therefore to rely exclusively
504 on the WAGASCI module information alone to reconstruct, identify and measure the
505 momentum of pions or protons.
- 506 • the coverage of the MRDs is not 4π . Using the WAGASCI module information can
507 therefore help to constraint the particles that exits the WAGASCI module but do
508 not geometrically enters any MRD.
- 509 • the particle identification of low momenta muons $p_\mu < 300$ MeV/c that will leave only
510 few hits in the MRD. Using the WAGASCI module information will clearly enhance

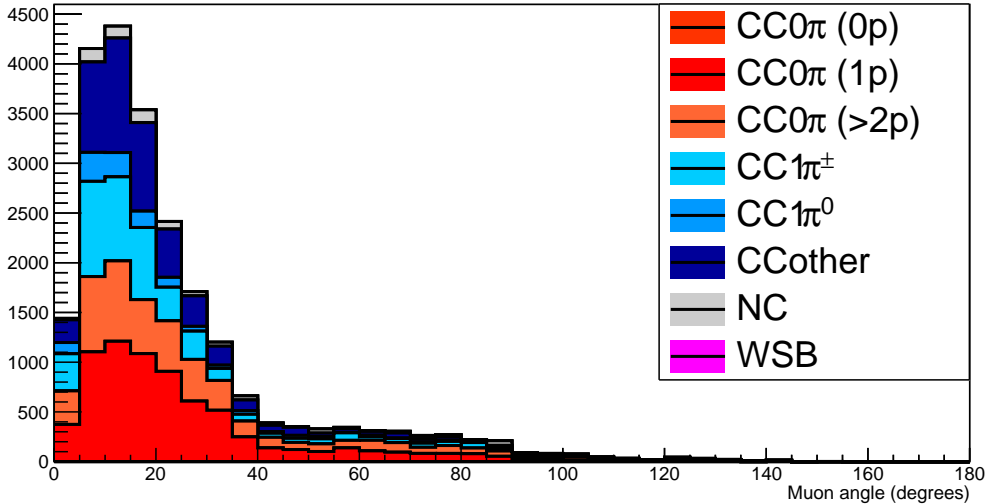


Figure 24: The reconstructed angles of the longest tracks in the selected events in the neutrino-mode.

511 the particle identification.

512 This study is based on an original study done for the ND280 upgrade target, with some
 513 modifications. Though the cell size is similar to the WAGASCI configuration presented
 514 in Section ??, the external dimensions are different ($186.4 \times 60 \times 130 \text{ cm}^3$). Whenever
 515 the results are presented with this external size and this parameter is likely to impact the
 516 result, it will be mentioned.

517 Note that in this section, a simplified reconstruction algorithm presented in Section ?? is
 518 used. The fiducial volume is chosen accordingly as the inner cube of the module which
 519 surfaces are distant of $4 \times$ scintillator space = 10 cm from the module external surfaces.

520 The neutrino interactions are simulated using NEUT v5.3.2. The NEUT input neutrino
 521 flux is estimated using JnuBeam v13a and assuming the detector to be located at 1.5° off-
 522 axis, as in Section ???. Note that the event reconstruction efficiency as a function of true
 523 neutrino energy might be changed at 1.5° , due for example to different Q^2 distributions. For
 524 this reason, one has to note that the reconstruction results might slightly be changed from
 525 2.5° and 1.5° . To avoid a similar change on the particle-only reconstruction efficiencies,
 526 they will be presented as a function of variables that completely characterize the particle
 527 kinematic state, *i.e.* its momentum and angle. Figure ?? shows the vertices distributions
 528 of the daughter particles of neutrinos interacting one standard WAGASCI water-module.

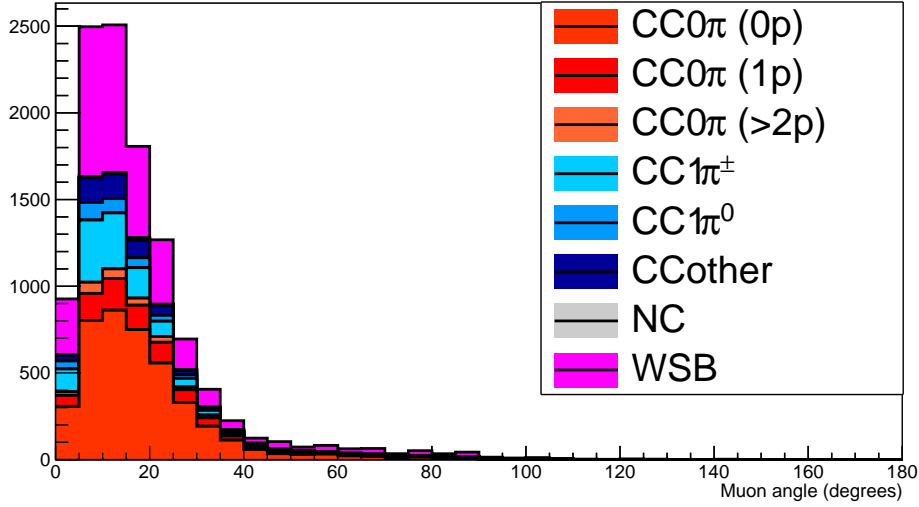


Figure 25: The reconstructed angles of the longest tracks in the selected events in the antineutrino-mode.

529 In this section, we will show the detector reconstruction and particle identification in this
 530 phase space, both for leptonic and hadronic particles. We will finally show an empty
 531 WAGASCI module can highly enhance the ability to constrain the neutrino interaction
 532 final state which is critical to reduce the corresponding uncertainties.

533 **6.1 Reconstruction algorithm**

534 **6.1.1 Description**

535 For this section, an ideal “simulated” reconstruction is developed. A particle is recon-
 536 structed if:

- 537 1. The particle is charged.
 538 2. Lets at least one hit (energy deposit > 2.5 photo-electron) in a scintillator.
 539

540 3. The particle enters one TPC and let one hit in the tracker.
 541 Or

- 542
- 543 • The particle should be long enough to be reconstructed by the detector in at
 544 least 2 out of 3 views (XZ, YZ, XY). The length criterion requires the particle

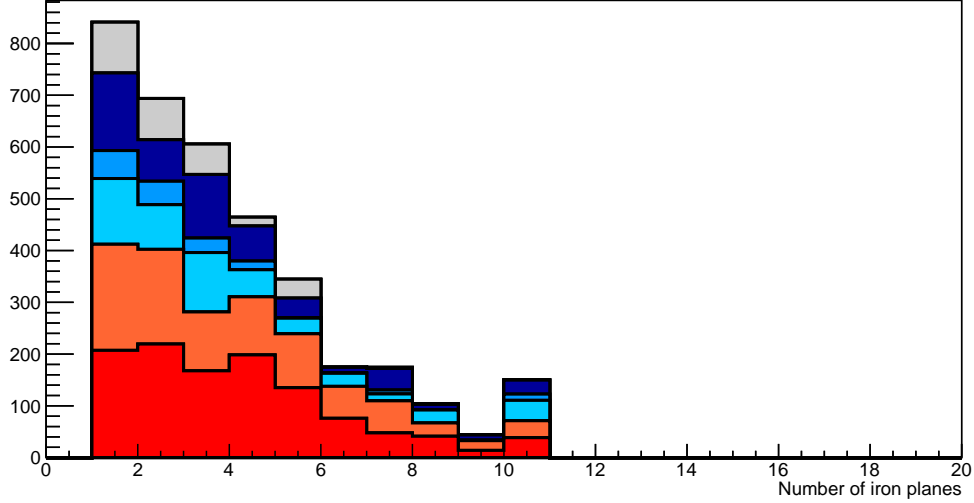


Figure 26: Iron plane numbers in Side-MRD corresponding to the end points of the longest tracks in the selected events in the neutrino-mode.

545 to let at least 4 hits in the detector. In the “less favourable case” of pure
 546 longitudinal or transverse going tracks, it represents a the track length of $L_{track} \geq$
 547 $4 \times$ scintillator space = 10.0 cm.

- 548 • In the views where particles pass the length criterion, the particle shall not
 549 be superimposed with longer tracks in at least two views. The superposition
 550 criterion is estimated with the distance inter-tracks (DIT) which corresponds to
 551 the orthogonal distance between two tracks at the ending point of the shortest
 552 one (see Figure ??). For a track 1, the superposition criterion is tested with
 553 every longer tracks that starts at the same vertex. Let \vec{p}_1 the vector of track
 554 1, and p_1^a its projections in the XZ, YZ and XY planes respectively for $i=1,2,3$.
 555 Note that these are projections in a 2D planes and not on a direction vector. In
 556 this case, the relative angle between the track 1 and a longer track 2 (of vector
 557 \vec{p}_2) in a view a is given by:

$$\cos \theta = \frac{\vec{p}_1^a \cdot \vec{p}_2^a}{\|\vec{p}_1^a\| \|\vec{p}_2^a\|} \quad (1)$$

558 and the distance inter track is given by:

$$DIT = \|\vec{p}_1^a\| \sin \theta \quad (2)$$

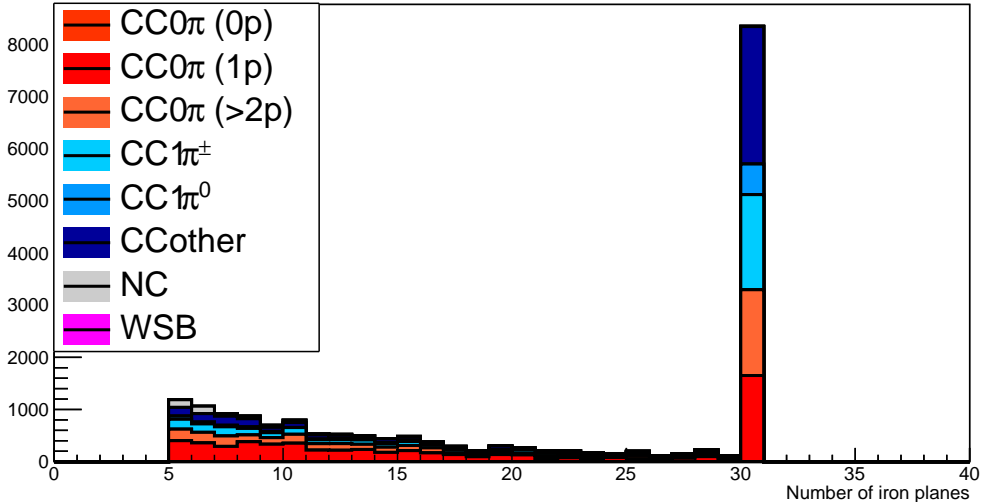


Figure 27: Iron plane numbers in Baby-MIND corresponding to the end points of the longest tracks in the selected events in the neutrino-mode.

559 The DIT should be higher than $4 \times$ scintillator width for the track 1 to be not
 560 superimposed with the track 2 in the view a, which also corresponds to 10.0 cm
 561 in the nominal configuration.

562 6.1.2 Performances

563 The particle-only reconstruction efficiencies and the reconstruction threshold in momenta
 564 are shown in Table ???. This threshold is defined as the maximal momentum for which the
 565 reconstruction efficiency is smaller than 30%. The thresholds in muon and pion momenta
 566 are 150 MeV/c. Most of the muons are above this threshold (see Figure ???) which leads
 567 to a 79% reconstruction efficiency.

568 The lower pion and proton efficiencies (respectively 52% and 26%) are due to lower
 569 efficiencies for similar momenta than muons, coming from strong interactions as shown
 570 on Figures ???. Efficiencies of each particle type tend to decrease in the backward region
 571 due to particle lower momenta. However, for a fixed momentum value, the reconstruc-
 572 tion efficiency is almost uniform which confirms the ability of the WAGASCI detector to
 573 reconstruct high angle tracks.

574 The reconstruction is thereafter tested on neutrino events. Table ?? summarizes the
 575 number of reconstructed events and efficiencies for each interaction type. As expected from

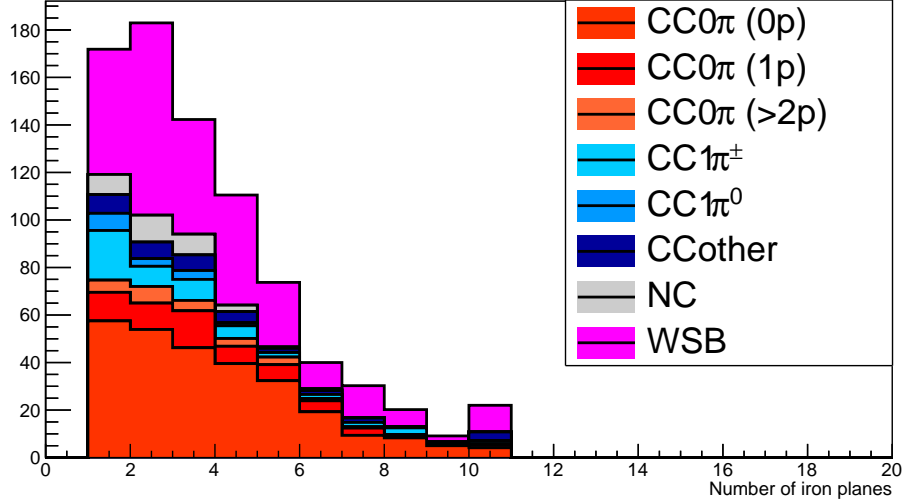


Figure 28: Iron plane numbers in Side-MRD corresponding to the end points of the longest tracks in the selected events in the antineutrino-mode.

	μ	π	p
Reconstruction Efficiency Momentum threshold	79% 150 MeV/c	52% 150 MeV/c	26% 550 MeV/c

Table 7: Reconstruction efficiency and momentum threshold for muons, pions and protons. The threshold is defined as the maximal momentum for which particles have a reconstruction efficiency smaller than 30%.

576 the high muon reconstruction efficiency, the charged current interactions have reconstruc-
577 tion efficiencies $\geq 85\%$.

578 The reconstruction efficiencies as a function of the neutrino energy and muon kinematics
579 are respectively shown on Figure ?? and ??.

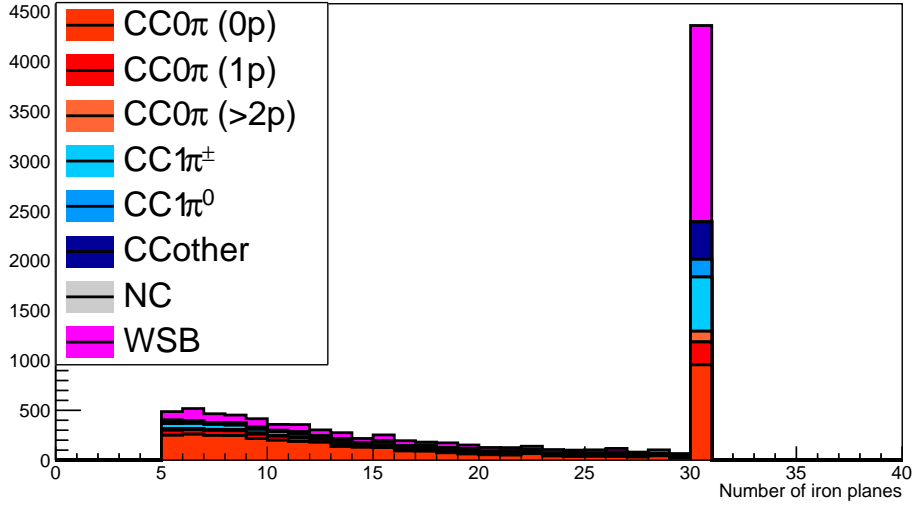


Figure 29: Iron plane numbers in Baby-MIND corresponding to the end points of the longest tracks in the selected events in the antineutrino-mode.

	CC0π	CC1π	CCOthers	NC	All
Reconstruction efficiency	85%	87%	91%	22%	68%

Table 8: Number of true interactions reconstructed. The purity and reconstruction efficiency of each true interaction is also shown.

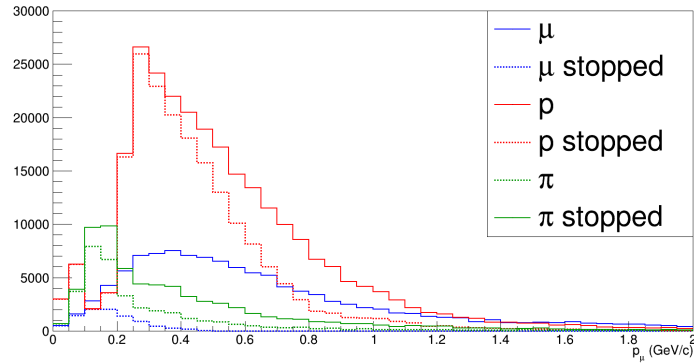


Figure 30: Momentum distribution of true particles in WAGASCI (plain) and corresponding distributions only for particles stopping into the WAGASCI module (dashed).

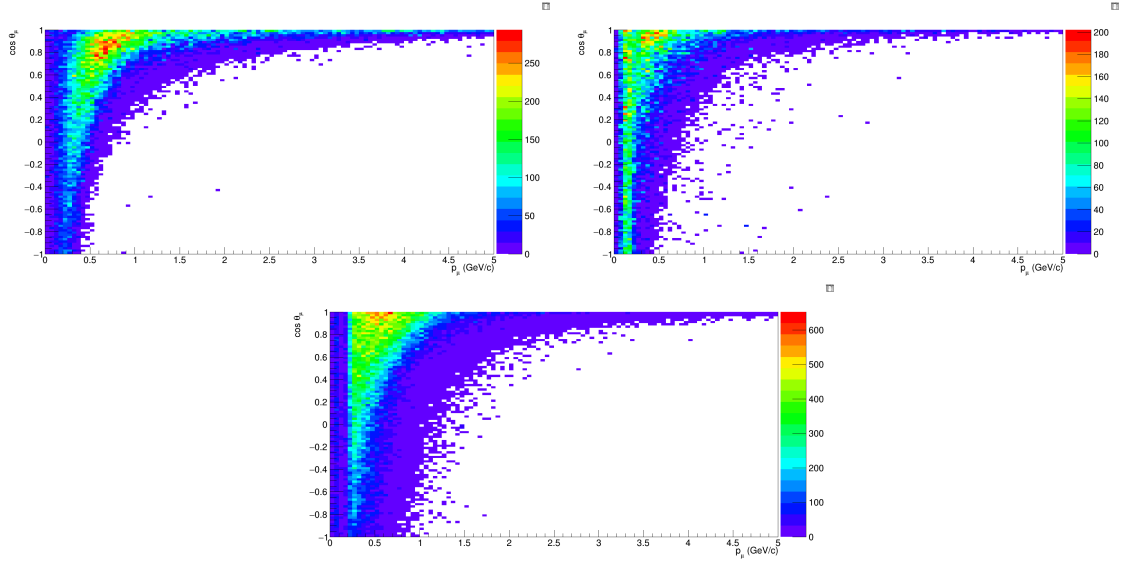


Figure 31: True number of muons (left), charged pions (right) and protons (bottom) in the two WAGASCI water-module as a function of the particles momenta and angles at 1.5° .

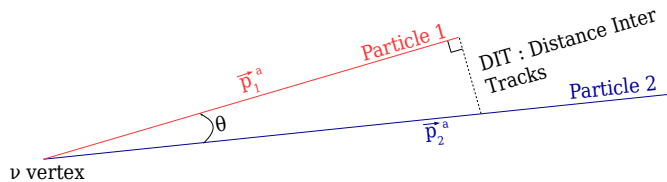


Figure 32: Definition of the distance inter tracks.

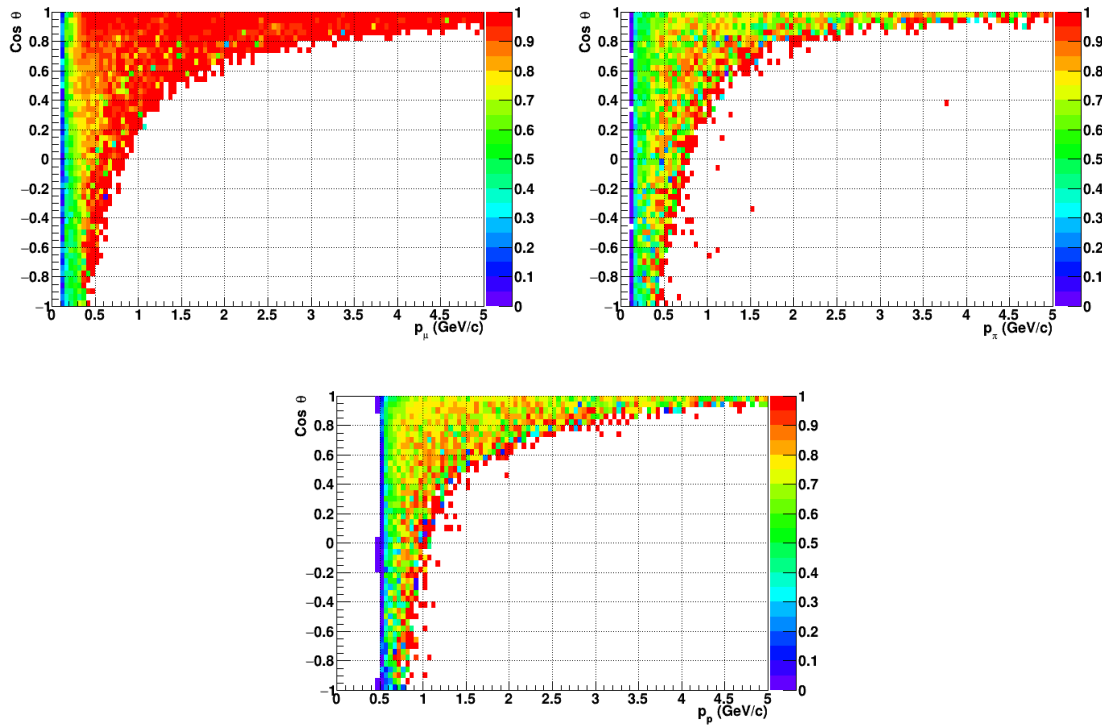


Figure 33: Reconstruction efficiency of muons (left), charged pions (right) and protons (bottom) in the WAGASCI water-module as a function of the particles momenta and angles.

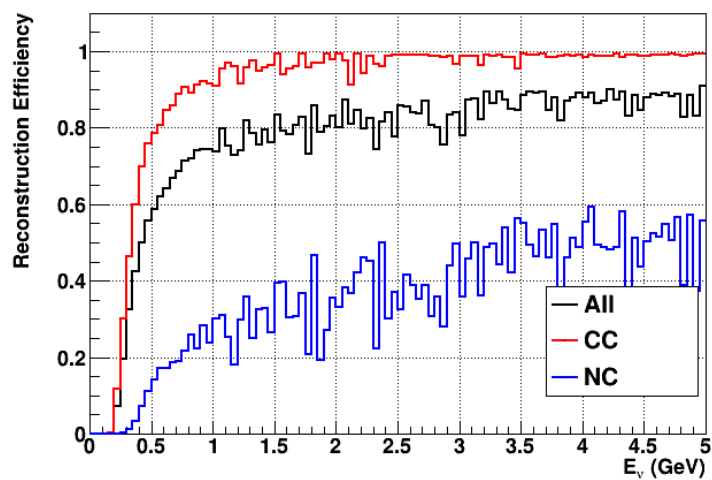


Figure 34: Reconstruction efficiency of all neutrino (black), CC (red) and NC (blue) interactions in the WAGASCI water-module as a function of the neutrino energy.

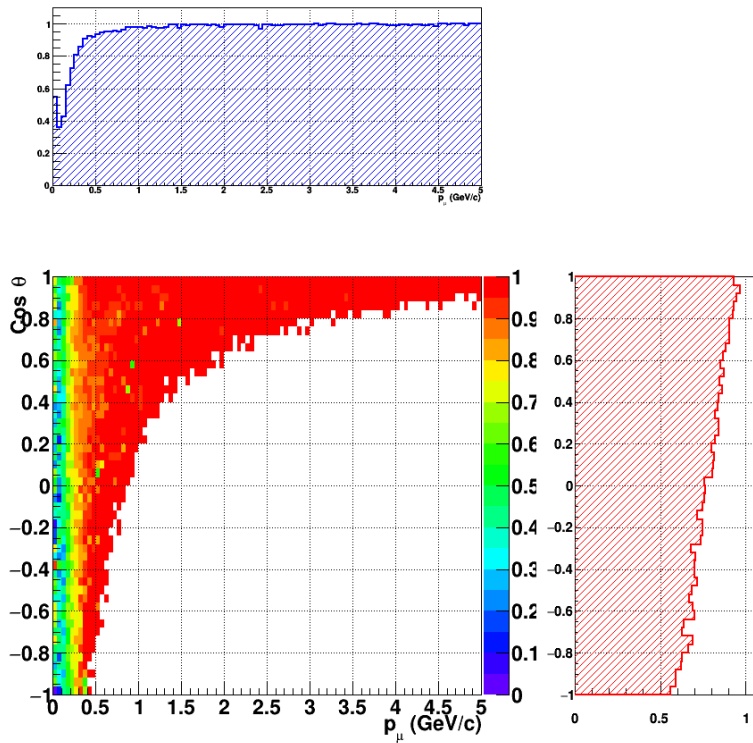


Figure 35: Reconstruction efficiency of CC interactions in the WAGASCI water-module as a function of the muon kinematic variables (momentum and angle).

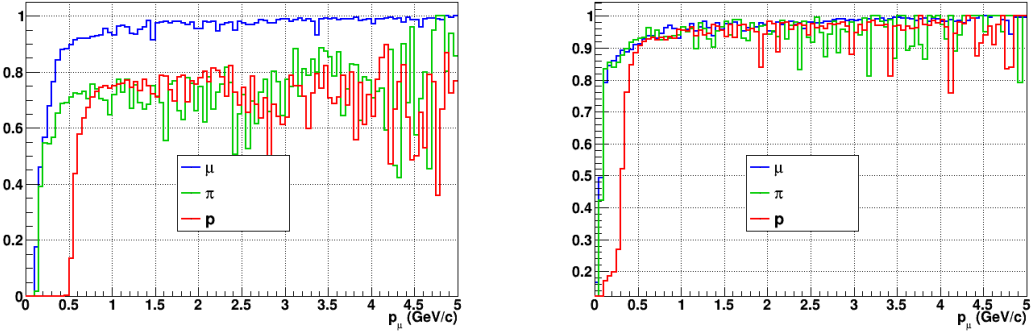


Figure 36: Reconstruction efficiency for muons, pions and protons in the water-in (left) and water-out (right) modules.

Note that a Particle Identification Algorithm has been also developed. It is based on the charge deposition of the particles in the scintillator, of the detection of a decay-electron. However, this information highly depends on the number of scintillator hit by a particle, which creates an important difference between a real WAGASCI module and the one used for the ND280-upgrade simulation. For this reason, the corresponding results will not be detailed here, but can be found in [?].

6.2 Background subtraction: the water-out module

In the nominal configuration, 20% of the neutrino interactions occurs on scintillators (C_8H_8). This background should be removed in order to measure the neutrino interaction on the same target as Super-K, which suppress the differences in cross-section models. For this purpose, we propose to use a water-out module, where the water is replaced by air. The detector is therefore fully active and has a 3 mm spatial resolution (scintillator thickness) which create an ideal detector to reconstruct and identify hadrons, and study np-nh interactions. The counter-part is the difference in particle energy deposition between the water and this water-out module that will need to be corrected for. In this section, we present the capabilities of such a module, and the impact it can have on cross-section measurements for the neutrino community in general and T2K in particular. The same reconstruction and selection as the water-in module is applied. Figure ?? shows the comparison between the water-in and the water-out reconstruction efficiencies for muon, pions and protons. 90% of the muons and 87% of the pions are reconstructed, while 70% of the protons are even reconstructed. It allows to lower down the proton threshold to 250 MeV/c (see Table ??).

As a consequence of tracking even low momenta particle, the reconstruction efficiency is uniform and almost maximal on the entire $\cos \theta_\mu$ phase space, as shown on Figure ??.

	μ	π	p
Reconstruction Efficiency Momentum threshold	90% 50 MeV/c	87% 50 MeV/c	70% 250 MeV/c

Table 9: Reconstruction efficiency, proportions of μ -like and non μ -like and momentum threshold for muons, pions and protons in the empty module. The threshold is defined as the maximal momentum for which particles have a reconstruction efficiency smaller than 20%.

604 Since the fiducial mass represents 0.25 tons, the total number of events is divided by a
 605 factor of 3 compared to the water-in module. The water-out module offers interesting
 606 possibilities to study np-nh interaction since 70% of the protons are reconstructed. In the
 607 future, a possible separation as a function of the number of proton track will be studied.
 608 Moreover, we are currently pursuing the use of single and double transverse variables (cite
 609 Xianguo) to open new possibilities for separating np-nh from Final State Interactions, or
 610 for isolating the interactions on hydrogen from interactions on carbon in this module.

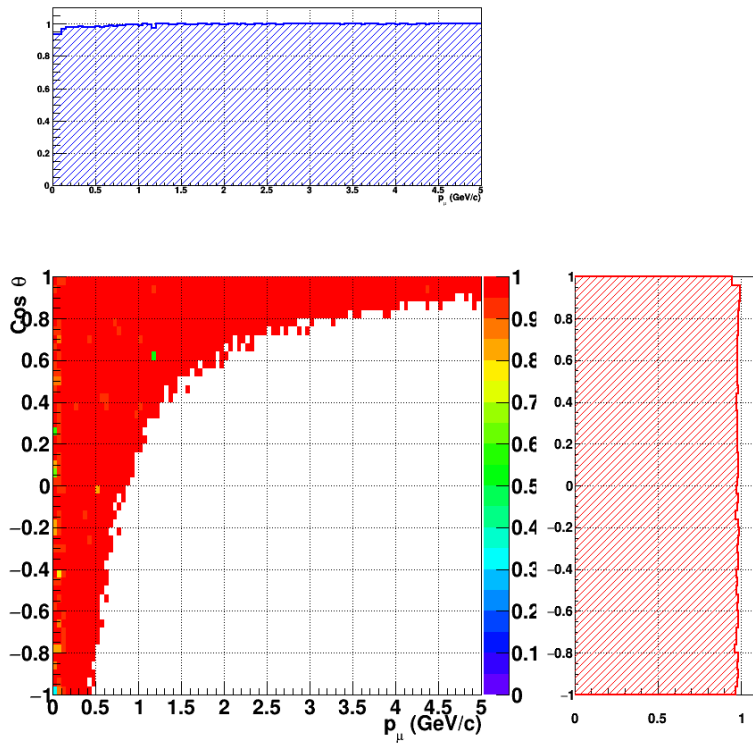


Figure 37: Reconstruction efficiency of CC interactions in the WAGASCI empty module as a function of the muon kinematic variables (momentum and angle).

611 **7 Schedule**

612 We would like to start a physics data taking from T2K beam time after the summer
613 shutdown in 2018. By then, commissioning and tests of the detectors will be completed
614 in J-PARC T59. The experiment can run parasitically with T2K, therefore we request no
615 dedicated beam time nor beam condition as discussed in the following section.

616 Once the approved POT is accumulated, the WAGASCI modules will be removed
617 from the experimental site, but we would like to keep the Baby-MIND and the Side-MRD
618 modules on the B2 floor of the NM pit as common platforms of future neutrino experiments
619 using the T2K neutrino beam.

620 **8 Requests**

621 **8.1 Neutrino beam**

622 The experiment can run parasitically with T2K, therefore we request no dedicated beam
623 time nor beam condition. As data taking periods, we request the ‘nominal’ T2K one-year
624 operation both for the neutrino beam and the antineutrino beam. The T2K has been
625 requesting 0.9×10^{21} POT/year and actually accumulating about 0.7×10^{21} POT/year in
626 recent years. For each year, starting from the Autumn, T2K is running predominantly in
627 the neutrino mode or in the antineutrino mode. Our request is to have one-year neutrino-
628 mode data and another one-year antineutrino mode data assuming that the POT for the
629 fast extraction in each year is more than 0.5×10^{21} POT.

630 **8.2 Equipment request including power line**

631 We request the followings in terms of equipment on the B2 floor:

- 632 • Site for the WAGASCI modules, Side-MRD modules and BabyMIND and their elec-
633 tronics system on the B2 floor of the near detector hall (Fig. ??).
- 634 • Anchor points (holes) on the B2 floor to secure the WAGASCI modules, Side-MRD
635 module and Baby-MIND (Fig. ??)
- 636 • Power line for the magnets in Baby-MIND: 400 V tri-phase 48-to-62 Hz, capable of
637 delivering 12 kW.
- 638 • Electricity for electronics and water circulation system, 3 kW, standard Japanese
639 electrical sockets.
 - 640 1. Online PCs: 2.1 kW
 - 641 2. Electronics: 0.7 kW
 - 642 3. Water sensors: ?

- 643 • Air conditioner for cooling heat generation at Baby-MIND magnets, online PCs and
644 electronics
- 645 • Beam timing signal and spill information
- 646 • Network connection

647 **8.2.1 Baby MIND Equipment request including power line**

648 We request the following in terms of equipment on the B2 floor:

- 649 • Site for the Baby MIND detector and its electronics systems on the B2 floor of the
650 near detector hall.
- 651 • Anchor points (holes) on the B2 floor to secure the 9 support frames, of order 4 holes
652 per frame, detailed floor plans to be communicated in a separate document.
- 653 • Power line for the magnet: 400 V tri-phase 48-to-62 Hz, capable of delivering 12
654 kW. We have a wish for the magnet power line to be installed and available to us by
655 beginning of March 2018.
- 656 • Electricity for electronics, 1 kW, standard Japanese electrical sockets.
- 657 • Beam timing signal and spill information
- 658 • Network connection

659 The infrastructure for much of the above exists already, and will be shared in part with
660 the WAGASCI experiment. Exceptions are the power line for the magnet and holes in the
661 B2 floor to anchor the detector support structures.

662 **9 Conclusion**

663 **References**

- 664 [1] K. Abe et al. Measurement of the muon neutrino inclusive charged-current cross sec-
665 tion in the energy range of 13 GeV with the T2K INGRID detector. *Phys. Rev.*,
666 D93(7):072002, 2016.
- 667 [2] M. Antonova et al. Baby MIND Experiment Construction Status. In *Prospects in*
668 *Neutrino Physics (NuPhys2016) London, London, United Kingdom, December 12-14,*
669 *2016*, 2017.
- 670 [3] K. Nitta et al. The k2k scibar detector. *Nucl. Instrum. Meth. A*, 535:147, 2004.

- 671 [4] J. Fleury, S. Callier, C. de La Taille, N. Seguin, D. Thienpont, F. Dulucq, S. Ahmad,
672 and G. Martin. Petiroc and Citiroc: front-end ASICs for SiPM read-out and ToF
673 applications. *JINST*, 9:C01049, 2014.
- 674 [5] M. B. Barbaro J. A. Caballero T. W. Donnelly G. D. Megias, J. E. Amaro. Inclusive
675 electron scattering within the susav2 meson-exchange current approach. *Phys. Rev. D*,
676 94:013012, 2016.
- 677 [6] Yu. G. Kudenko, L. S. Littenberg, V. A. Mayatsky, O. V. Mineev, and N. V. Ershov.
678 Extruded plastic counters with WLS fiber readout. *Nucl. Instrum. Meth.*, A469:340–
679 346, 2001.
- 680 [7] O. Mineev, Yu. Kudenko, Yu. Musienko, I. Polyansky, and N. Yershov. Scintillator
681 detectors with long WLS fibers and multi-pixel photodiodes. *JINST*, 6:P12004, 2011.
- 682 [8] Etam Noah et al. Readout scheme for the Baby-MIND detector. *PoS*, Pho-
683 toDet2015:031, 2016.